Article

Developmental Cell

Leukocyte Cytoskeleton Polarization Is Initiated by Plasma Membrane Curvature from Cell Attachment

Graphical Abstract

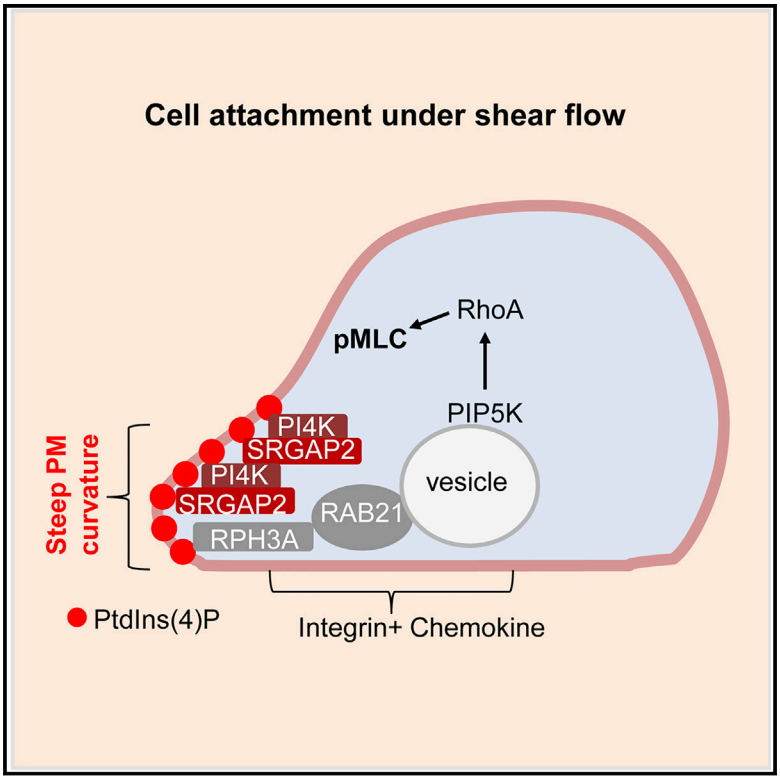

Authors

Chunguang Ren, Qianying Yuan, Martha Braun, ..., Erdem Karatekin, Wenwen Tang, Dianqing Wu

Correspondence

erdem.karatekin@yale.edu (E.K.), wenwen.tang@yale.edu (W.T.), dan.wu@yale.edu (D.W.)

In Brief

The molecular mechanisms controlling cell polarization are incompletely understood. Ren and Yuan et al. show that local increase in plasma membrane (PM) curvature resulting from cell attachment recruits and polarizes an inverse FBAR domain protein SRGAP2 to initiate cell cytoskeleton polarization, which is important for neutrophil adhesion to endothelium.

Highlights

- Cell attachment is required for chemical-induced cytoskeleton polarization
- Cell attachment induces local PM curvature increase to recruit and polarize SRGAP2
- Polarized SRGAP2 induces sequential polarization of PtdIns4P, PIP5K1C90, and pMLC
- This SRGAP2 polarization signaling axis regulates neutrophil firm adhesion

Ren et al., 2019, Developmental Cell *49*, 1–14
April 22, 2019
https://doi.org/10.1016/j.devcel.2019.02.023

CellPress

Please cite this article in press as: Ren et al., Leukocyte Cytoskeleton Polarization Is Initiated by Plasma Membrane Curvature from Cell Attachment, Developmental Cell (2019), https://doi.org/10.1016/j.devcel.2019.02.023

Developmental Cell
Article

Leukocyte Cytoskeleton Polarization Is Initiated by Plasma Membrane Curvature from Cell Attachment

Chunguang Ren,[1,16] Qianying Yuan,[1,16] Martha Braun,[2,3,14] Xia Zhang,[4] Björn Petri,[5,6] Jiasheng Zhang,[7] Dongjoo Kim,[8] Julia Guez-Haddad,[9] Wenzhi Xue,[10] Weijun Pan,[10] Rong Fan,[8] Paul Kubes,[5,11] Zhaoxia Sun,[12] Yarden Opatowsky,[9] Franck Polleux,[13] Erdem Karatekin,[2,3,14,15,*] Wenwen Tang,[1,*] and Dianqing Wu[1,17,*]

[1]Department of Pharmacology, Vascular Biology and Therapeutic Program, Yale University, New Haven, CT 06520, USA
[2]Department of Cellular and Molecular Physiology, Yale University, New Haven, CT 06520, USA
[3]Nanobiology Institute, Yale University, New Haven, CT 06520, USA
[4]Department of Geriatrics, the First affiliated Hospital, College of Medicine, Zhejiang University, Hangzhou, Zhejiang, China
[5]Snyder Institute for Chronic Diseases Mouse Phenomics Resource Laboratory, University of Calgary, Calgary AB T2N 4N1, Canada
[6]Department of Microbiology, Immunology, and Infectious Diseases, University of Calgary, Calgary AB T2N 4N1, Canada
[7]Department of Internal Medicine, Yale University, New Haven, CT 06520, USA
[8]Department of Biomedical Engineering, Yale University, New Haven, CT 06520, USA
[9]The Mina & Everard Goodman Faculty of Life Sciences, Bar-Ilan University, Ramat-Gan 5290002, Israel
[10]Shanghai Institute of Nutrition and Health, Shanghai Institutes for Biological Sciences, University of Chinese Academy of Sciences, Chinese Academy of Sciences (CAS), Shanghai, China
[11]Department of Physiology and Pharmacology, Cumming School of Medicine, and Calvin, Phoebe, and Joan Snyder Institute for Chronic Diseases, University of Calgary, Calgary AB T2N 4N1, Canada
[12]Department of Genetics, Yale University, New Haven, CT 06520, USA
[13]Department of Neuroscience, Mortimer B. Zuckerman Mind Brain Behavior Institute, Columbia University, New York, NY 10025, USA
[14]Department of Molecular Biophysics and Biochemistry, Yale School of Medicine, Yale University, New Haven, CT 06520, USA
[15]Centre National de la Recherche Scientifique (CNRS), Paris, France
[16]These authors contributed equally
[17]Lead Contact
*Correspondence: erdem.karatekin@yale.edu (E.K.), wenwen.tang@yale.edu (W.T.), dan.wu@yale.edu (D.W.)
https://doi.org/10.1016/j.devcel.2019.02.023

SUMMARY

Cell polarization is important for various biological processes. However, its regulation, particularly initiation, is incompletely understood. Here, we investigated mechanisms by which neutrophils break their symmetry and initiate their cytoskeleton polarization from an apolar state in circulation for their extravasation during inflammation. We show here that a local increase in plasma membrane (PM) curvature resulting from cell contact to a surface triggers the initial breakage of the symmetry of an apolar neutrophil and is required for subsequent polarization events induced by chemical stimulation. This local increase in PM curvature recruits SRGAP2 via its F-BAR domain, which in turn activates PI4KA and results in PM PtdIns4P polarization. Polarized PM PtdIns4P is targeted by RPH3A, which directs PIP5K1C90 and subsequent phosphorylated myosin light chain polarization, and this polarization signaling axis regulates neutrophil firm attachment to endothelium. Thus, this study reveals a mechanism for the initiation of cell cytoskeleton polarization.

INTRODUCTION

Cell migration plays an important role in many biological contexts including embryonic development, wound healing, tumor metastasis, and particularly various aspects of leukocyte biology including leukocyte infiltration, recruitment, trafficking, and homing (de Oliveira et al., 2016; Nourshargh and Alon, 2014; Kolaczkowska and Kubes, 2013; Ley et al., 2007). Before a cell can migrate, it has to polarize through spatial reorganization of signaling and structural molecules. Cell polarization is not only necessary for migration but also confers the directionality of the migration. Primary neutrophils, neutrophil-like cell lines, and *Dictyostelium* are popular models for studying directional cell migration induced by the gradient of a chemoattractant, which was also known as chemotaxis. Those cells form polarized cytoskeleton structures including lamellar F-actin at the leading edge (the front) and actomyosin at the uropod (the back) upon chemoattractants stimulations. The formation of lamellar F-actin at the front is primarily driven by chemoattractant-activated small GTPase RAC proteins, whereas PIP3-linked mechanisms help to localize, consolidate, and stabilize F-actin polymerization. Chemoattractants also stimulate small GTPase RHOA activation and myosin light chain phosphorylation (pMLC) and induce their localizations at the back of the cell. This "back" polarization, which underlies the formation of the actomyosin structure or uropod, may provide pushing force for cell locomotion but

Please cite this article in press as: Ren et al., Leukocyte Cytoskeleton Polarization Is Initiated by Plasma Membrane Curvature from Cell Attachment, Developmental Cell (2019), https://doi.org/10.1016/j.devcel.2019.02.023

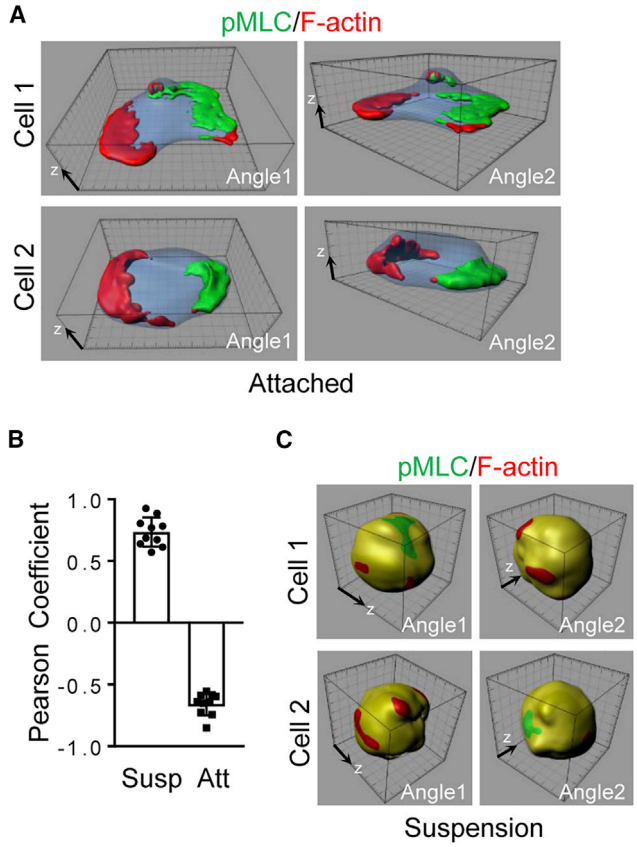

Figure 1. Neutrophil Polarization Requires Cell Attachment

(A–C) Mouse neutrophils attached on fibrinogen (Fn)-coated coverslips (A) or suspended in a microtube (C) were stimulated uniformly with MIP2 (100 nM) for 3 min at room temperature. Cells were stained with Alexa633-phalloidin (for staining F-actin) and anti-pMLC followed with an Alexa488-secondary antibody and observed with a confocal microscope. Reconstructed 3D images of two representative cells per condition are shown. The 3D raw images of Cell 1 in (A) and Cell 1 in (C) are shown as Videos S1 and S2, respectively. Quantification of colocalization of pMLC and F-actin is also shown in (B). Each data point represents a cell. The experiments were repeated three times. The grid scales in (A) and (C) are 1 μm.

See also Figure S1.

is more important for neutrophil firm adhesion to the endothelium during infiltration (Hind et al., 2016; Devreotes and Horwitz, 2015; Nichols et al., 2015; Xu and Jin, 2015; Graziano and Weiner, 2014; Majumdar et al., 2014; Woodham and Machesky, 2014; Tang et al., 2011; Cramer, 2010; Insall, 2010; Xu et al., 2010; Sánchez-Madrid and Serrador, 2009; Wang, 2009; Gómez-Moutón and Mañes, 2007; Ridley et al., 2003).

While chemoattractants act through their G-protein-coupled receptors to provide a chemical input in cell polarization regulation, integrin signaling, as another extracellular chemical input, can also confer neutrophils polarity in the absence of any chemoattractant by inducing Pip5k1c90 polarization (Xu et al., 2010). During *in vivo* infiltration, circulating naive neutrophils are captured by integrin-mediated adhesion after selectin-mediated rolling, before they are stimulated by chemoattractants (Kolaczkowska and Kubes, 2013; Ley et al., 2007). Pip5k1c is one of three PIP5K1 molecules that are responsible for phosphatidylinositol(4,5)-bisphosphate ($PtdIns4,5P_2$) synthesis in most cells (Clarke et al., 2007). This PIP5K1C90 polarization has important impacts on chemoattractant-induced polarization and chemotaxis. It is not only important for polarized RHOA activation and pMLC polarization at the uropods but also to determine the initial cellular polarity, which chemoattractant-induced polarization has to follow initially (Tang et al., 2011).

It is noteworthy that most of the studies of cell polarization initiated by chemical stimulation (chemoattractant and/or integrin) were done with cells that had already attached to surfaces. Stochastic polarity was suspected to exist in the attached cells, which, in combination with positive feedback circuitry and self-organizing capability of macromolecules such as polymerized actin and myosin and microtubules, was used to explain spontaneous or uniform stimulation-induced cellular polarization (Ladoux et al., 2016; Woodham and Machesky, 2014; Asnacios and Hamant, 2012; Altschuler et al., 2008; Sohrmann and Peter, 2003). In this study, we demonstrate that extracellular chemical stimulation is insufficient for breaking cellular symmetry or initiating cytoskeleton polarization in neutrophils. Instead, local increase in plasma membrane (PM) curvature, which results from cell contact to a surface, initiates the breakage of cellular symmetry through polarized localization of an F-BAR-containing protein SRGAP2 and subsequent PM PtdIns4P. These PM-curvature-induced polarization events supersede those induced by chemoattractants and integrins.

RESULTS

Attachment Is Required for Neutrophil Polarization

When neutrophils were stimulated with a chemoattractant, the chemoattractant not only stimulated the formation of F-actin and phosphorylation of MLC, it also caused polarization of F-actin and pMLC (Figures 1A, 1B, and S1A). Namely, the newly formed lamellar F-actin was localized at one end, whereas pMLC was at the other end of a cell. This is a well-documented phenomenon observed in mouse, human, and zebrafish neutrophils regardless of uniform or gradient chemoattractant stimulations (Gao et al., 2015; Record et al., 2015; Lam et al., 2014; Kumar et al., 2012; Liu et al., 2010; Shin et al., 2010; Xu et al., 2010; Shi et al., 2009; Subramanian et al., 2007; Wong et al., 2007; Francis et al., 2006; Van Keymeulen et al., 2006; Bodin and Welch, 2005; Xu et al., 2005; Srinivasan et al., 2003; Xu et al., 2003; Seveau et al., 2001). However, we realized that such polarization events had only been examined and reported in cells that had been attached to a surface. When we treated mouse neutrophils suspended in physiological media with MIP2, neither F-actin nor pMLC showed polarized localization. Instead, F-actin and pMLC were largely colocalized (Figures 1B, 1C, and S1B). The same result was also observed with fMLP stimulation of mouse neutrophils (data not shown) and CXCL12 stimulation of mouse primary $CD8^+$ T cells (Figure S1C). Thus, we concluded that cell attachment was a previously unrealized prerequisite for these polarization events in neutrophils stimulated by chemoattractants.

SRGAP2 Is Important for pMLC Polarization

We hypothesized that cell attachment results in alteration in PM curvature, which may be a cue for neutrophil polarization. The

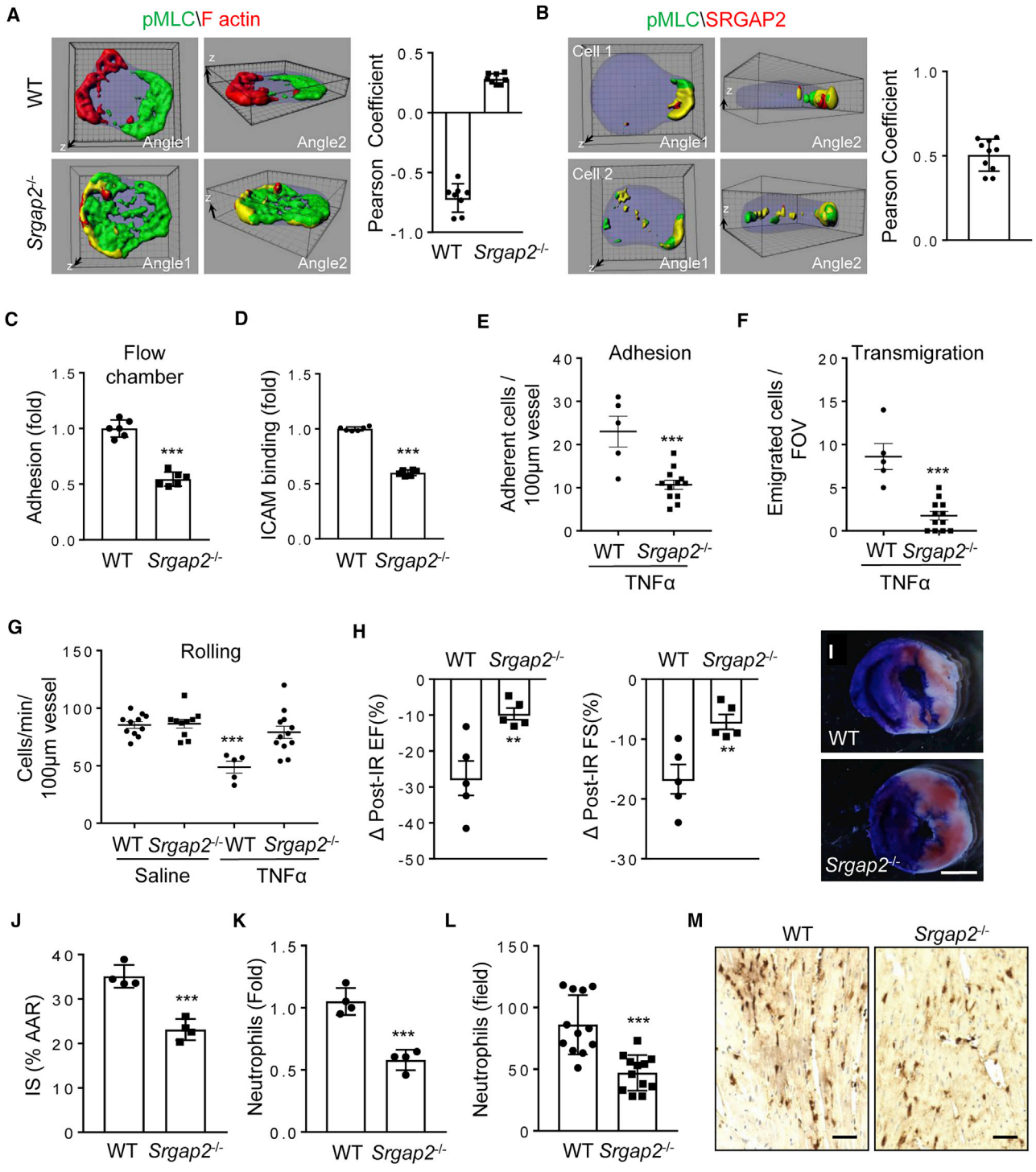

Figure 2. Importance of SrGAP2 in Neutrophil Polarization and Adhesion

(A) SRGAP2 deficiency disrupts pMLC polarization. WT or Srgap2$^{-/-}$ neutrophils were stimulated and examined for F-actin and pMLC localization as in Figure 1A. Each data point represents a cell. The experiments were repeated three times.

(B) SRGAP2 is co-polarized with pMLC in stimulated neutrophils. Neutrophils were stimulated as in Figure 1A and examined for SRGAP2 and pMLC localization by immunostaining with anti-pMLC and anti-SRGAP2 (C14), followed by Alexa488 (green)- and Alexa633 (red)-conjugated secondary antibodies, respectively. Reconstructed 3D confocal images of two representative cells per condition are shown. Each data point represents a cell.

(C and D) SRGAP2 deficiency impairs neutrophil attachment to endothelial cell under shear flow (C) and ICAM1 binding (D). Each data point represents a biological replicate. The experiments were repeated three times.

(legend continued on next page)

Bin-Amphiphysin-Rvs (BAR)-domain-containing proteins are known to sense and induce PM curvature (Simunovic et al., 2015; Suetsugu et al., 2010; Frost et al., 2009). We thus performed siRNA screening of BAR-domain-containing genes that are expressed in mouse neutrophils based on gene expression analysis. We found that silencing of the *Srgap2* (Slit-Robo-GTPase activating protein 2) gene, but not any of other five BAR-domain-containing genes, disrupted polarized localization of pMLC upon chemoattractant stimulation (Figure S2A). We confirmed the importance of SRGAP2 in pMLC polarization by observing defective pMLC polarization in neutrophils isolated from SRGAP2-deficient mice (Figures 2A and S2B–S2D). In addition, the SRGAP2 protein and pMLC were co-polarized at the same side of activated neutrophils (Figures 2B and S2E). None of these BAR-domain-containing proteins including Srgap2, however, appeared to be involved in F-actin polarization (Figures 2A and S2C; data not shown).

SRGAP2 Is Important for Neutrophil Adhesion

While SRGAP2 deficiency did not grossly alter chemotactic behaviors of neutrophils under a chemoattractant gradient in a Dunn chamber (Figure S2F), it reduced neutrophil adhesion to endothelial cells in a flow chamber assay (Figure 2C). Concordantly, SRGAP2-deficient neutrophils showed decreased binding of ICAM1 (Figure 2D). Moreover, SRGAP2-deficient neutrophils exhibited impaired adhesion to wild-type (WT) endothelia in an intravital microscopic observation of blood vessels in inflamed cremaster muscles (Figure 2E). There was also a reduction in the number of transmigrated SRGAP2-deficient neutrophils and a lack of TNFα-induced reduction in the number of rolling Srgap2$^{-/-}$ cells in the inflamed vessels (Figures 2F and 2G), which could be the result of the reduction in neutrophil adhesion.

We next adopted the cardiac ischemia-reperfusion (IR) model to evaluate if SRGAP2 plays a significant role in neutrophil recruitment in a disease model (Hoyer and Nahrendorf, 2017; Vinten-Johansen, 2004). We generated hematopoietic-loss of SRGAP2 by transferring Srgap2$^{-/-}$ bone marrow into lethally irradiated WT recipient mice. The lack of SRGAP2 in hematopoietic cells ameliorated IR injuries to the hearts by lessening IR-induced changes in percentage of ejection fraction (EF) and fractional shortening (FS) (Figures 2H and S2G), decreasing the infarction areas (Figures 2I, 2J, and S2H) and reducing the infiltration of neutrophils into the injured cardiac tissues (Figures 2K–2M and S2I). Of note, SRGAP2 deficiency does not affect the number of various leukocytes in circulation (Table S1). Although these results do not prove that SRGAP2 deficiency ameliorates IR-induced cardiac injury exclusively via impairment of neutrophil adhesion and recruitment, they clearly demonstrate an impairment of neutrophil recruitment by SRGAP2 deficiency in an *in vivo* pathophysiological model. In addition, these cardiac IR phenotypes are consistent with the impairment of neutrophil adhesion and recruitment. Putting all of the data together, we conclude that SRGAP2 regulates pMLC polarization and has an important role in neutrophil adhesion to endothelial cells and recruitment *in vivo*.

SRGAP2 Regulates RAB21, RPH3A, and PIP5K1C90 Polarization

We have previously characterized a pathway that directs polarization of PIP5K1C90 via directional transport of RAB21 vesicles (Yuan et al., 2017). Polarized PIP5K1C90 is required for polarized RhoA activation and pMLC localization (Xu et al., 2010). In addition, neutrophils lacking PIP5K1C90 show similar adhesion phenotypes to those of SRGAP2-null neutrophils (Xu et al., 2010). Together with the observation that SRGAP2 and PIP5K1C90 were polarized to the same side of stimulated neutrophils (Figure S3A), we decided to examine if SRGAP2 regulates PIP5K1C90 and RAB21 polarization in neutrophils. The lack of SRGAP2 significantly reduced the number of neutrophils exhibiting polarized localization of PIP5K1C90 or RAB21 (Figures 3A and 3B). Of note, in our preparation of primary neutrophils, there were about 20% of cells that failed to respond to any stimulation regardless of assays (migration, polarization, etc.) likely because of the lack of maturity or poor cell health status.

In our previous study, we also identified RPH3A as an effector of RAB21, which is required for targeting the RAB21 vesicles to their final polarized destinations, even though how RPH3A directs the polarized vesicle transport remained unknown (Yuan et al., 2017). While RPH3A deficiency had no effect on SRGAP2 polarization (Figure S3B), SRGAP2 deficiency disrupted RPH3A polarization (Figure 3C). These results, together with the co-polarization of SRGAP2 and RPH3A at the same side of neutrophils (Figure 3D), suggest that SRGAP2 may be a direct or indirect target for RPH3A and guides RPH3A-associated RAB21 vesicles to their polarized destination.

PM PtdIns4P Shows Polarized Localization in Neutrophils

The simplest possibility would be that RPH3A binds to SRGAP2 to serve as a direct target. However, we could not detect this interaction using a number of approaches including

(E–G) SRGAP2-null neutrophil showed impaired attachment to endothelium in inflamed cremaster muscle venues. Lethally irradiated WT mice received either WT or *Srgap2*$^{-/-}$ bone marrow transfer and were subjected to intravital examination 2 months later. Adhesion (E), transmigration of neutrophils (F), and rolling flux (G), were determined after stimulation of the cremaster muscle with TNFα (0.5 μg) for 4 h. Two-tailed Student's t test and two-way ANOVA test were performed for (E), (F), and (G), respectively. Each data point represents the observation with one vessel. Three mice were used for each condition.

(H–J) SRGAP2 deficiency ameliorates ischemia-reperfusion (IR) injury in the heart. Mice receiving WT or Srgap2$^{-/-}$ bone marrows were subject to IR injury. Changes in percentage of ejection fraction (EF %) and fractional shortening (FS %) are shown. Representative images (I) and quantification (J) of infarction areas are also shown. Area at risk (AAR) are identified as the Evans blue stain negative area, whereas infarct size (IS) as the white area within AAR. Each point represents an individual mouse. The experiments were repeated three times and representative results were shown in (H)–(J).

(K–M) SRGAP2 deficiency decreases neutrophil infiltration in the injured heart tissues as determined by flow cytometry (K) or quantification of histological images stained with an anti-Ly-6B.2 antibody (L). Representative image of Ly-6B.2-stained sections are shown (M). Each data point in (J) and (K) represents an individual mouse. Each data point in (L) represents a random imaging field from one section within a similar location of the heart (12 fields from 4 mice). The experiments were repeated three times and representative results were shown in (K)–(M). Scale bars are 1 mm (I) and 0.1 mm (M). The grid scales in (A) and (B) are 1 μm. See also Figure S2.

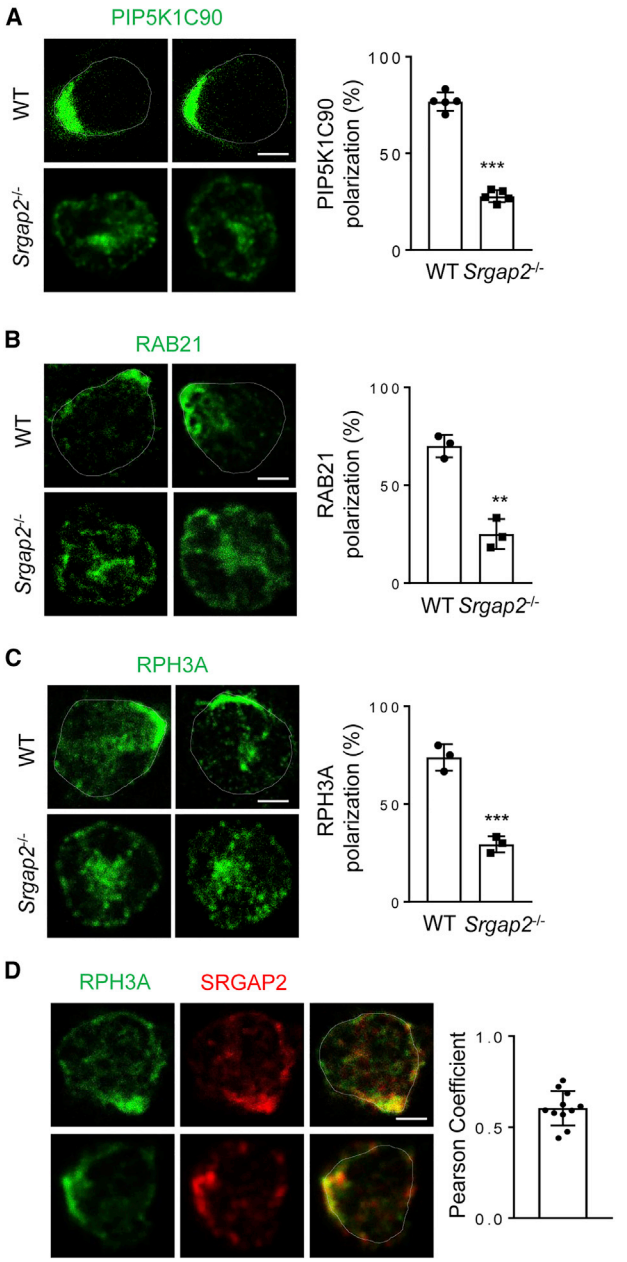

Figure 3. SRGAP2 Regulates PIP5K1C90, RAB21, and RPH3A Polarization

(A–C) SRGAP2-deficiency impairs PIP5K, RAB21, and RPH3A polarization. Neutrophils were stimulated as in Figure 1A and stained by anti-PIP5K1C90 (A), anti-RAB21 (B), or anti-RPH3A (C), followed by an Alexa488-conjugated second antibody before being imaged by confocal microscopy. Representative optical section images of two cells from each genotype are shown. Quantification of polarization was performed as described in the STAR Methods. Each data point represents the average of more than 10 cells per observation field, and the experiment was repeated three times.

(D) Co-polarization of RPH3A and SRGAP2 in neutrophils. Neutrophils were stimulated as in Figure 1A before being stained with anti-RPH3A and anti-SRGAP2 (G10) antibodies, followed with Alexa488 (green)- and Alexa633 (red)-conjugated secondary antibodies, respectively. Representative optical section images of two cells are shown. Each data point represents a cell. The experiments were repeated three times. Scale bars are 3 μm.

See also Figure S3.

co-immunoprecipitation in overexpressed cells and pull-down assays using recombinant proteins (data not shown). It is thus possible that there might be an intermediate(s) between SRGAP2 and RPH3A. RPH3A contains C2 domains, which are known to bind to phosphatidylinositol (PtdIns) lipids (Corbalan-Garcia and Gómez-Fernández, 2014). Our characterization of RPH3A-PtdIns interactions indicated that RPH3A preferentially bound to PtdIns4P (Figure 4A). Lipid binding was assessed using a liposome floatation assay (Zhang et al., 2013; Boswell et al., 2012), in which liposomes with a composition similar to the inner leaflet of the PM were used. In addition, Ca^{2+} enhanced this binding (Figure 4A), which is a common characteristic of C2 domains (Rizo and Südhof, 1998). Because the F-BAR domain of SRGAP2 can bind to PtdIns4P (Coutinho-Budd et al., 2012), we decided to investigate if PtdIns4P has a role in neutrophil polarization.

Despite the abundance of PtdIns4P in the Golgi (De Matteis et al., 2013), this lipid has been detected in other intracellular locations including PM (De Matteis et al., 2013; Hammond et al., 2012; Jethwa et al., 2012; Nakatsu et al., 2012; Hammond et al., 2009). We tested the role of PM PtdIns4P in neutrophil polarization by employing a method reported by Hammond et al. (2012). In this system, rapamycin induces rapid recruitment of active sac1 (an *S. cerevisiae* phosphatase for PtdIns4P) fused to the FKBP protein (designated as FKBP-SAC) to PM-anchored Lyn_{11}-FRB to specifically hydrolyze PM PtdIns4P (Figure S4A). FKBP-SAC- and mCherry-tagged Lyn_{11}-FRB plasmids were electroporated at 5:1 ratio into neutrophils, which were subsequently separated into the fluorescence-positive and -negative populations by fluorescence-activated cell sorting (FACS). Given the plasmid ratio in transfection, most of the fluorescent cells should contain FKBP-SAC, and rapamycin should induce PM PtdIns4P depletion in these cells. Even though some of the fluorescence-negative cells may also contain FKBP-SAC, they cannot respond to rapamycin without the PM anchor and thus were used as the control. We validated the depletion system by staining the neutrophils with an anti-PtdIns4P antibody (Hammond et al., 2012). The antibody detected two obvious pools of signals in the control cells; one is co-localized with the Golgi marker TGN38, whereas the other is non-Golgi and proximal to PM (Figure S4B). The PM-PtdIns4P depletion system specifically diminished the non-Golgi pool without affecting the Golgi pool, suggesting that the non-Golgi pool is likely the PM PtdIns4P pool (Figure S4B). This experiment additionally validated the antibody-based PtdIns4P detection system and more importantly revealed that PM PtdIns4P showed polarized localization in stimulated neutrophils. Furthermore, we found that PtdIns4P was co-polarized with RPH3A and SRGAP2 at the same side of stimulated neutrophils (Figures 4B and 4C).

PM PtdIns4P Is Important for Neutrophil Polarization

We next examined the impact of PM PtdIns4P depletion on neutrophil polarization. PM PtdIns4P depletion significantly impaired polarized localization of RPH3A (Figure 4D), PIP5K1C90 (Figure S4C), RAB21 (Figure S4D), or pMLC (Figure S4E). In addition, depletion of PM PtdIns4P also resulted in reductions in firm adhesion of neutrophils to endothelial cells under shear flow and neutrophil ICAM binding (Figure 4E), the same phenotypes observed for inactivation of SRGAP2 (Figures 2C

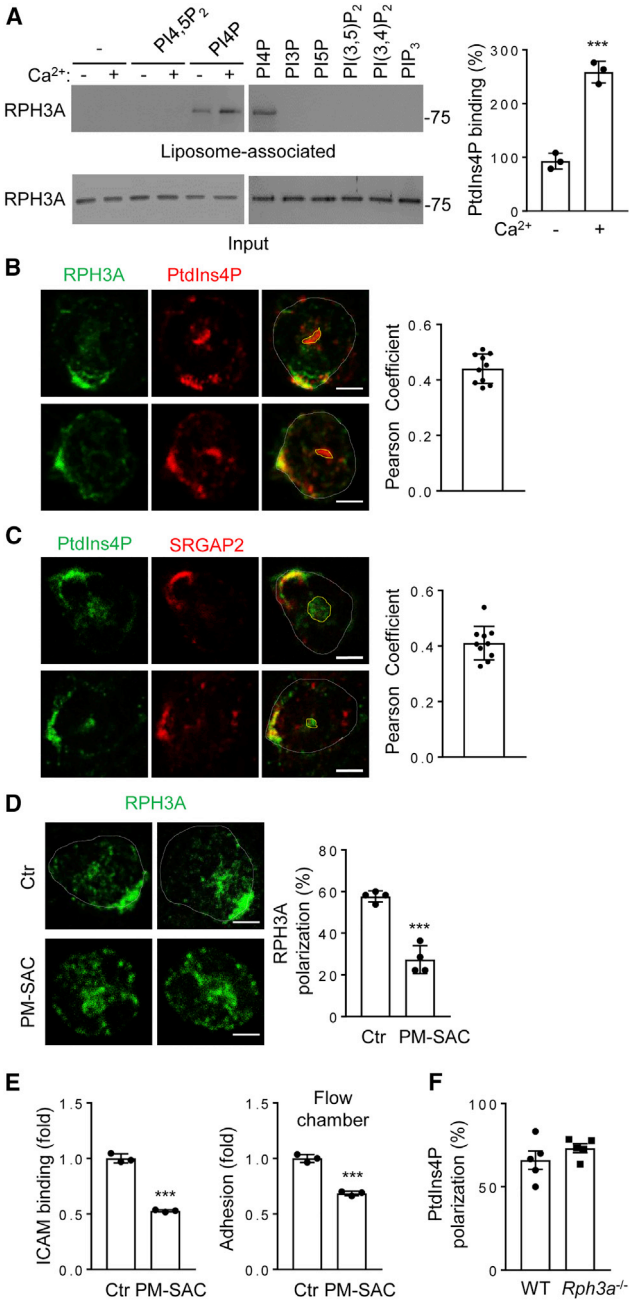

and 2D), RAB21, RPH3A, or PIP5K1C (Yuan et al., 2017; Xu et al., 2010). Thus, these data together indicate that PM PtdIns4P has an important role in polarization of PIP5K1C90, RAB21, RPH3A, and pMLC. Consistent with our hypothesis that PM PtdIns4P may be the target for RPH3A-directed polarization, RPH3A-deficiency did not affect PtdInd4P polarization in neutrophils (Figure 4F). Moreover, depletion of PtdIns4,5P_2 using the system described by Hammond et al. (2012) did not affect PIP5K1C90 polarization (Figure S4F), while PtdIns4P depletion did not affect Ptdins3,4,5P3 contents or polarization (Figure S4G) (Kwon et al., 2007). These results further affirm the conclusion that PtdIns4P, rather than other PtdIns lipids, plays a key role in the PIP5K1C polarization axis.

SRGAP2 Regulates PM PtdIns4P Polarization

Although PM PtdIns4P depletion affects many of the polarization events described above, it did not affect SRGAP2 polarization (Figure 5A). However, SRGAP2 deficiency impaired PtdIns4P polarization in neutrophils (Figure 5B), suggesting that SRGAP2 may act upstream of PtdIns4P polarization. Re-expression of WT SRGAP2 or its GAP-activity-deficient mutant, but not the F-BAR-domain-lacking mutant, restored PtdIns4P polarization impaired by SRGAP2 knockdown in neutrophils (Figure S5A). These results, together with colocalization of SRGAP2 with PtdIns4P (Figure 4C), suggest that SRGAP2 may regulate PtdIns4P polarization. Among the four PtdIns kinases that can convert PtdIns to PtdIns4P, silencing of PI4KA, but not others, significantly affected the detection of polarized PM PtdIns4P (Figures 5C, 5D, and S5B). In fact, PI4KA silencing reduced PM PtdIns4P content without affecting Golgi PtdIns4P content (Figures 5C, 5E, and 5F), whereas PI4KB and PI4K2A knockdown reduced Golgi PtdIns4P contents (Figures 5C and 5F). PI4KA silencing also impaired pMLC polarization without affecting F-actin polarization (Figure S5C), and its effects on PM PtdIn4P polarization and content could be rescued by co-expression of human PI4KA (Figure S5D). Moreover, we found that PI4KA and SRGAP2 co-immunoprecipitated (Figure S5E) and that SRGAP2 could stimulate the lipid kinase activity of PI4KA in an *in vitro* kinase assay (Figure S5F). These results together provide a mechanism for SRGAP2 to polarize PM PtdIns4P. Namely, polarized localization of SRGAP2 stimulates polarized formation of PtdIns4P, while the interaction of SRGAP2 with PtdIns4P (Coutinho-Budd et al., 2012) may help to stabilize PtdIns4P polarization and serve as a possible feedforward-local amplification mechanism by recruiting additional SRGAP2,

Figure 4. RPH3A Binds to and Polarizes Downstream of PtdIns4P

(A) RPH3A binds to PtdIns4P but not other PtdIns lipids as determined by the liposome flotation assay. Calcium (100 μM) was present as indicated and in the right panel. The experiments were repeated three times. The quantification of RPH3A binding to PtdIns4P in the presence or absence of Ca^{2+} is shown.

(B and C) Co-polarization of RPH3A (B) or SRGAP2 (C) with PtdIns4P. Neutrophils were stimulated as in Figure 1A before being co-stained with anti-RPH3A or anti-SRGAP2 (C14) with anti-PtdIns4P antibodies, followed by Alexa488 (green)- and Alexa633 (red)-conjugated secondary antibodies as indicated in the figure. Representative optical section images of two cells are shown. The PtdIns4P stain encircled in yellow denotes the Golgi pool. Each data point represents a cell. The experiments were repeated three times.

(D) Depletion of PtdIns4P impairs polarization of RPH3A. Neutrophils were transfected with Lyn_{11}-FRB-mCherry and FKBP-SAC at 1:5 ratio and separated into mCherry positive (PM-SAC) and negative (Ctr) pools by FACS. These neutrophils were then stimulated as in Figure 1A in the presence of 1 μM rapamycin before being stained with anti-RPH3A and Alexa488-conjugated secondary antibody. Representative optical section images of two cells from each condition are shown. Each data point represents the average of more than 10 cells per observation field, and the experiment was repeated four times.

(E) PtdIns4P depletion impairs neutrophil attachment to endothelial cell under shear flow and ICAM1 binding. Each data point represents a biological replicate. The experiments were repeated three times.

(F) RPH3A-deficiency does not affect PtdIns4P polarization. Neutrophils were stimulated as in Figure 1A and stained with anti-PtdIns4P. Each data point represents the average of more than 10 cells per observation field, and the experiment was repeated five times. Scale bars in (B)–(D) are 3 μm.

See also Figure S4.

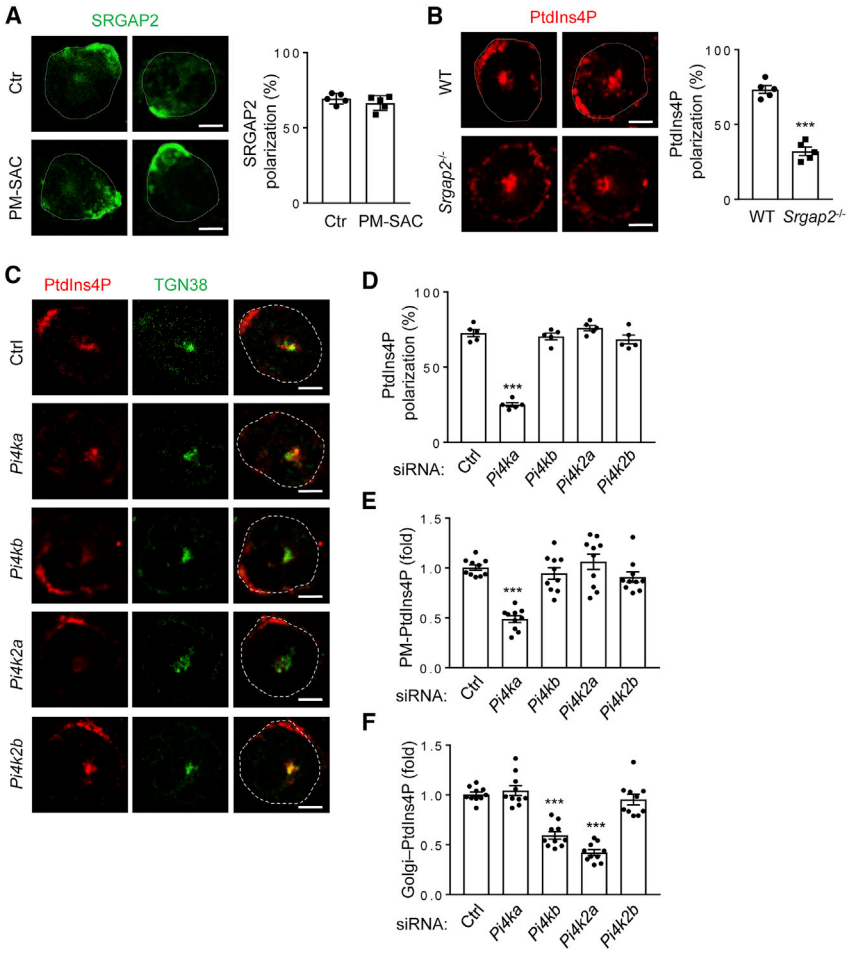

Figure 5. SRGAP2 Polarizes PtdIns4P via PI4KA

(A) PtdIns4P depletion does not impair polarization of SRGAP2. Neutrophils were transfected and treated as in Figure 4D before being stained with anti-SRGAP2 (G10) and Alexa488 conjugated secondary antibody. Representative optical section images of two cells from each condition are shown. Each data point represents the average of more than 10 cells per observation field, and the experiment was repeated five times.

(B) SRGAP2-deficiency impairs PtdIns4P polarization. Neutrophils were stimulated as in Figure 1A and stained with anti-PtdIns4P and Alexa633 conjugated secondary antibody. Representative optical section images of two cells from each genotype are shown. Each data point represents the average of more than 10 cells per observation field, and the experiment was repeated five times.

(C–F) PI4KA is involved in PtdIns4P polarization. Neutrophils were transfected with siRNAs for various PtdInsP kinases for 48 h and treated as in Figure 1A before being stained with anti-PtdIns4P and anti-TGN38 antibodies followed by Alexa633 (red) and Alexa488 (green) conjugated secondary antibodies, respectively. Representative confocal optical section images (C) and quantification of PtdIns4P polarization (D) and PM (E) or Golgi (F) PtdIns4P staining intensities are shown. The PM or Golgi PtdIns4P staining intensities are expressed as the ratios of PM or Golgi PtdIns4P to TGN38 staining. Each data point represents the average of more than 10 cells per observation field. Scale bars (A)–(C) are 3 μm.

See also Figure S5.

leading to further production of PtdIns4P. Now, the question is how SRGAP2 is polarized in neutrophils.

Attachment-Induced PM Curvature Polarizes SRGAP2

Freshly isolated neutrophils in suspension are spherical, but their attachment to a surface would results in a cell shape change, leading to local alteration in PM curvature. SRGAP2 contains an inverse F-BAR domain, which is recruited to concave curvatures of lipid membranes where it polymerizes and in turn helps to stabilize the curvatures (Sporny et al., 2017; Charrier et al., 2012; Guerrier et al., 2009). Together with our observation that SRGAP2 F-BAR domain is required for PtdIns4P polarization (Figure S5A), we hypothesized that a local increase in PM curvature around the attachment zone might recruit SRGAP2 via its inverse F-BAR domain. Indeed, while the F-BAR domain of SRGAP2 fused to EGFP (FBAR-GFP) showed non-polarized localization in neutrophils in suspension (Figure 6A), cells attached to a surface showed increased localization of FBAR-GFP at the cusps above the coverslip, resulting in dorsoventral polarization of FBAR-GFP (Figure 6B). In other words, more FBAR-GFP is localized ventrally than dorsally. Among these dorsoventrally polarized cells, nearly one-half also displayed noticeable anteroposterior polarization (Figures 6C and 6E). When polarization of FBAR-GFP was observed at real time, we noticed that the cells that showed anteroposterior polarization often had movements on the coverslip (probably because of lateral drifting prior to settling onto the surface) before they arrested on the surface (Figure S6A). Polarization intensified rapidly after the cell came to a stop with the polarization direction conforming to the prior movement direction (Figure S6A). We interpreted these results to suggest that cell-attachment-induced PM curvature increase recruits SRGAP2 to the cusps of cell attachment, leading to dorsoventral polarization of SRGAP2. On the other hand, cell movement on the surface due to lateral drifting results in steeper PM curvature at the trailing end of the cell as schemed in Figure S6A. The steeper PM curvature would have a higher affinity for SRGAP2, leading to anteroposterior polarization of SRGAP2. If this idea is correct, neutrophils subjected to shear flow, which they normally experience during their attachment to the endothelium during inflammation, would result in increased anteroposterior polarization, as the shear flow would cause even steeper PM curvature at the trailing end by pushing the cell body forward. Indeed, when neutrophils were subjected to shear flow in a flow chamber, there was a significant increase in the percentage of the cells showing anteroposterior polarization of FBAR-GFP (Figures 6D and 6E). Importantly, FBAR-GFP polarized in a direction coinciding with the flow direction (Figure 6D), a phenomenon we have also previously

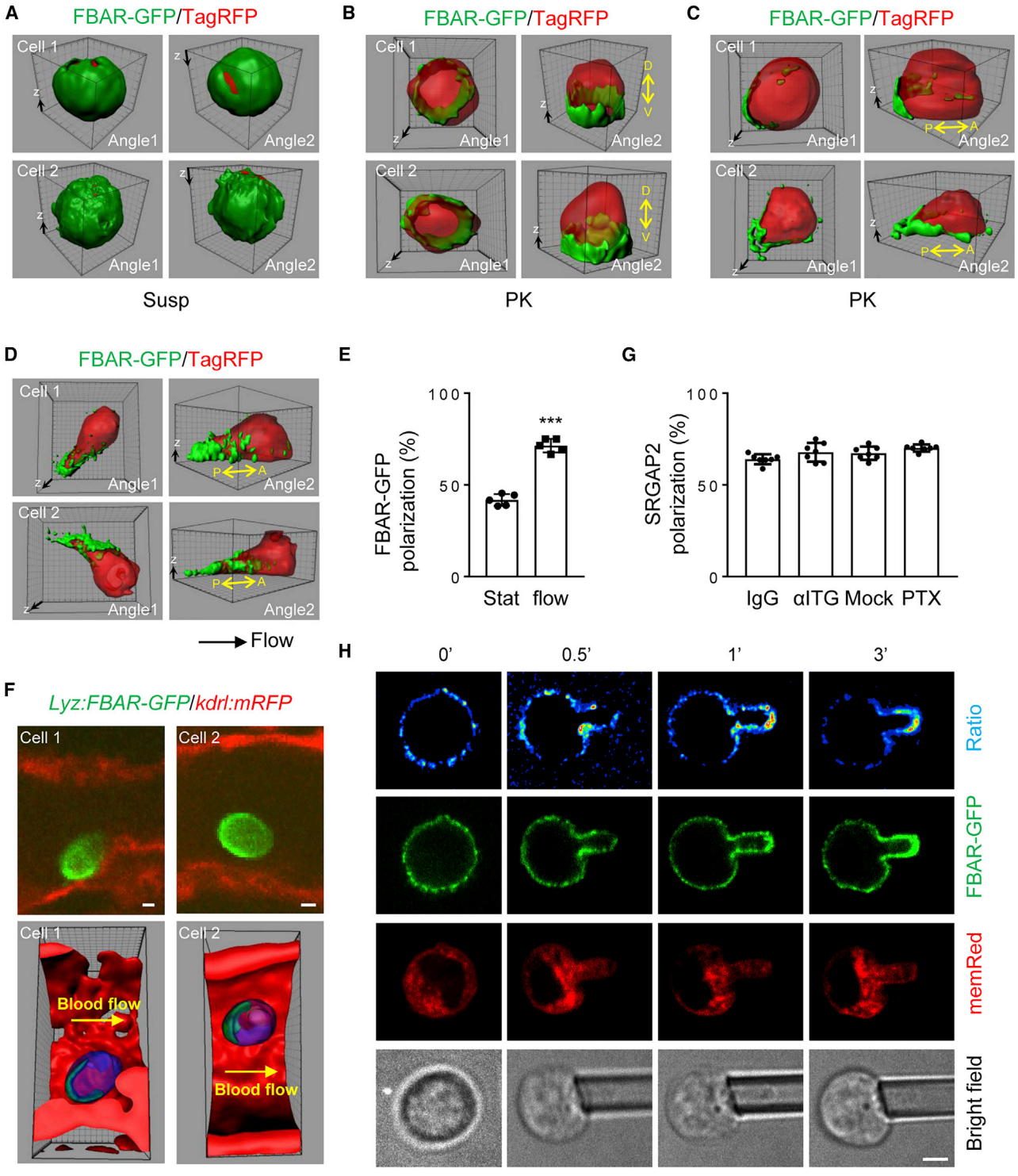

Figure 6. SrGAP2 F-BAR-domain Polarizes upon Attachment Independently of Chemical Stimulation

(A–C) SRGAP2 F-BAR-domain polarizes depending on cell attachment. Neutrophils were cotransfected with SrGAP2 F-BAR-domain-GFP (FBAR-GFP) and TagRFP for 6 h. They were either embedded in Hydrogel as suspended cells (A) or attached to PK-coated coverslips (B) and (C) for confocal microscopy. Representative 3D reconstructed images of two independent cells are shown. The 3D raw images are shown as Video S3 (Cell 1 in A), Video S4 (Cell 1 in B) and Video S5 (Cell 1 in C). Dorsal (D)-ventral (V) and anterior (A)-posterior (P) axes are denoted. The experiments were repeated three times.

(D and E) Shear flow promotes anteroposterior polarization. Neutrophils were cotransfected as in (A) and placed in a flow chamber with a PK-coated surface. The attached cells were subjected to shear flow (2 dyn/cm^2) for 10 min and imaged by a confocal microscope. Representative 3D reconstructed images of two

(legend continued on next page)

described for PIP5K1C90 polarization (Xu et al., 2010). Moreover, the GFP-fusion protein with I-Bar of IRSp53, F-Bar of FBP17, or N-Bar of Nadrin2 showed no polarization even under shear flow (data not shown). Furthermore, we observed FBAR-GFP polarization in neutrophils attached to inflamed blood vessels in live zebrafish in the direction of blood flow (Figure 6F).

It is important to note that the polarization of SRGAP2 FBAR-GFP described above occurred on poly-lysine (PK)-coated surfaces in the absence of exogenous chemoattractants or integrin ligands. We further confirmed the independence of FBAR-GFP polarization on chemoattractant or integrin signaling by pre-treating neutrophils with pertussis toxin (PTx) or a cocktail of integrin antibodies. As a validation, PTx treatment blocked MIP2-induced phosphorylation of AKT (Figure S6B), while the anti-integrin cocktail blocked RPH3A polarization (Figure S6C) and neutrophil spreading on fibrinogen (Fn) (Figure S6D). Neither pre-treatment, however, affected attachment-induced SRGAP2 polarization (Figure 6G). These results suggest that cell-attachment-induced SRGAP2 polarization is independent of chemoattractant or integrin signaling and may act upstream of chemoattractant signaling as chemoattractant failed to polarize neutrophils in suspension (Figures 1B and 1C).

To further test if changes in membrane curvature actually alter FBAR-GFP recruitment, we used micropipettes to aspirate single neutrophils in suspension to artificially create negative PM curvature (relative to the cytosol). FBAR-GFP was expressed in the neutrophils isolated from the mT/mG mouse (Muzumdar et al., 2007) that expressed membrane-associated TdTomato fluorescent protein (memRed; used as an internal control). Ratio images of FBAR-GFP to memRed were generated to more accurately assess FBAR-GFP PM localization. Upon aspiration, rapid increases of FBAR-GFP localization at the PM inside the micropipettes were observed (Figure 6H). Because the PM inside the micropipette has a higher concave curvature than the PM outside the micropipette, the above observation is consistent with our hypothesis diagramed in Figure S6A that increased PM curvature leads to efficient recruitment of FBAR-GFP and probably SRGAP2 via its F-BAR domain. We also carried out the aspiration experiment with micropipettes with different orifices, which led to different PM curvatures and quantified FBAR-GFP localization and membrane curvature as described in Figure S6E. We found a significant positive correlation of PM curvature with FBAR-GFP localization (Figures 6H and S6F). This provides further support for our hypothesis that within a certain range, the degree of PM curvature is correlated with FBAR-GFP recruitment.

We also divided the PM inside the pipette into two zones, the tip and tube zones (Figure S6E), and quantified them separately. There were significant positive correlations between PM curvature and FBAR-GFP localization in both zones (Figures S6G and S6H). Because the PM in the tip zone was not and might never have been in contact with any surface, this tip zone correlation result further affirms the conclusion that PM curvature rather than its contact with a surface recruits FBAR-GFP. On the other hand, PMs inside the tube zone are constrained by the pipette walls from forming membrane structures such as the filopodium or protrusion and likely have the same membrane tension. The significant positive correlation observed in this tube zone indicate that changes in membrane tension or formation of membrane structures such as the filopodium or protrusion are unlikely the primary mechanism for SRGAP2 F-BAR domain polarization in neutrophils. We also performed the same experiment with primary mouse $CD8^+$ T cells and observed similar results (Figures S6I and S6J). Taken together, our results indicate that a local increase in membrane curvature resulting from initial steps of cell attachment is the primary mechanism for polarization of FBAR-GFP and probably SRGAP2 in neutrophils, T cells, and probably other leukocytes.

Membrane Curvature Increase Drives PM PtdIns4P Polarization

Next, we wanted to determine if PM PtdIns4P polarizes as FBAR-GFP in a membrane curvature-dependent way but independently of chemoattractant or integrin stimulation. As we observed with FBAR-GFP, polarized localization of PtdIns4P was detected by the anti-PtdIns4P antibody in neutrophils placed on PK-coated surfaces, but not in cells in suspension (Figures S7A and S7B). We also detected PtdIns4P localization using a fluorescent PtdIns4P probe, GFP-P4M. P4M is a protein domain of the SidM protein from *L. pneumophila* that has a high affinity and specificity for PtdIns4P (Schoebel et al., 2010; Brombacher et al., 2009). GFP-P4M works faithfully as a PtdIns4P probe in live cells (Hammond et al., 2014). We co-expressed TagRFP (Navaroli et al., 2012) as an internal imaging control. PM GFP-P4M polarized in neutrophils attached to a PK-coated surface but not in cells in suspension (Figures 7A–7C). Similar to what we observed for FBAR-GFP, most of the GFP-P4M showed dorsoventral polarization at the cusps of cell attachment (Figure 7B), less than a half of which also showed anteroposterior polarization (Figures 7C and 7E). Shear flow increased the number of anteroposteriorly polarized cells (Figures 7D and 7E). Importantly, pre-treatment with either PTx, which blocks chemoattractant signaling, or the anti-integrin cocktail did not affect PM

independent cells are shown (D). The 3D raw images of Cell 1 in (D) are shown as Video S6. Each data point in E represents the average of more than 10 cells per observation field, and the experiment was repeated five times.

(F) SrGAP2 F-BAR-domain polarizes in inflamed blood vessels of zebrafish.

(G) PTx treatment or integrin neutralization has no effects on SRGAP2 polarization. Neutrophils were pre-treated with a control IgG, a cocktail of neutralizing integrin β1 and β2 antibodies (10 μg/mL), or pertussis toxin (PTx, 1 μg/mL for 2 h at 37°C) before being subjected to shear flow treatment as in (D) in a flow chamber with a PK-coated surface. Attached cells were stained with anti-SRGAP2 (G10) antibody and imaged by confocal microscopy. Cells showing anteroposterior polarization were scored. Each data point represents the average of more than 10 cells per observation field, and the experiment was repeated three times.

(H) Micropipette aspiration leads to polarization of the SrGAP2 F-BAR-domain to regions of high concave curvature (relative to the cytosol), namely along the pipette walls and the semi-spherical tip of the aspirated tongue. Membrane-associated TdTomato (memRed) expressing neutrophils from mT/mG mice were transfected with FBAR-GFP. Images of a representative cell are shown. The experiments were repeated ten times. Scale bars in (F) and (H) are 3 μm, and the grid scales in (A)–(D) are 1 μm.

See also Figure S6.

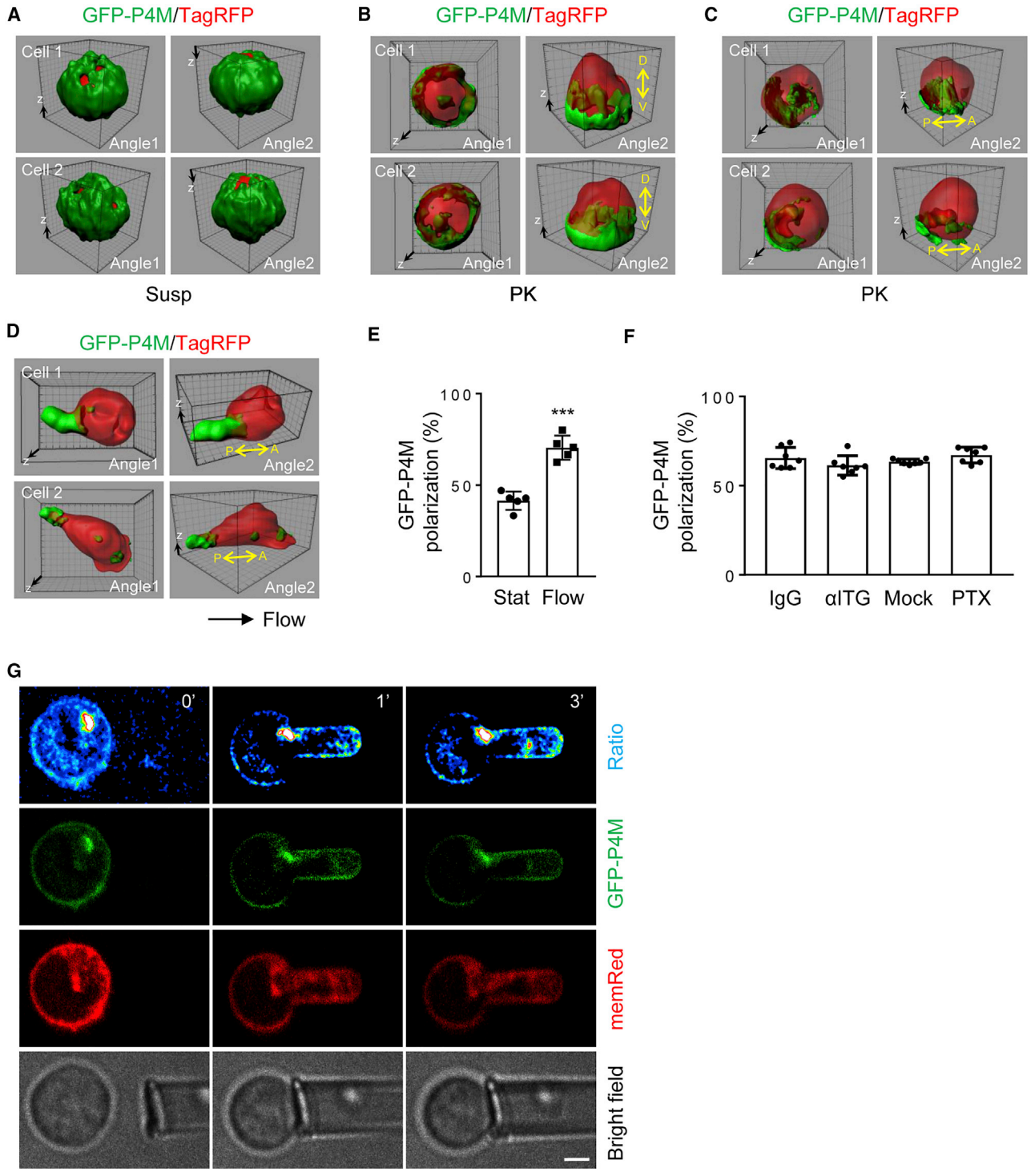

Figure 7. PM PtdIns4P Polarizes upon Attachment

(A–C) GFP-P4M polarizes depending on cell attachment. Neutrophils were cotransfected with GFP-P4M and TagRFP for 6 h. They were either embedded in hydrogel as suspended cells (A) or attached to PK-coated coverslips (B) and (C) for confocal microscopy. Representative 3D reconstructed images of two independent cells are shown. The experiments were repeated three times.

(D and E) Shear flow promotes anteroposterior polarization of GFP-P4M. Neutrophils were transfected and treated as in Figure 6D. Representative 3D reconstructed images of two independent cells are shown (D). Each data point in E represents the average of more than 10 cells per observation field, and the experiment was repeated five times.

(legend continued on next page)

GFP-P4M polarization in attached cells (Figure 7F). In cells coexpressing GFP-P4M and FBAR-TagRFP, these two proteins showed co-polarization to the same side of the cells (Figure S7C). Finally, we performed the micropipette aspiration experiment to induce controlled PM curvatures while monitoring PM PtdIns4P localization. When neutrophils expressing GFP-P4M and memRed were aspirated, as for FBAR-GFP, significant positive correlations of concave membrane curvatures to GFP-P4M localization were observed (Figures 7G and S7D–S7F). Thus, these results demonstrate that PM PtdIns4P, like SRGAP2 FBAR-GFP, polarizes upon cell attachment via local increase in PM curvature independently of chemoattractant or integrin signaling as depicted in Figure S7G.

DISCUSSION

In this study, we elucidate mechanisms by which an apolar neutrophil breaks its cellular symmetry to initiate cytoskeleton polarization. The initiation of leukocyte polarization had been assumed to be exclusively dependent on extracellular chemical stimulations including chemoattractants and integrins. We, however, show here that chemical stimulation alone is not sufficient for induction of polarization of lamellar F-actin and pMLC, two prominent cytoskeleton markers, in neutrophils in suspension. Neutrophil contact to a surface is a prerequisite for polarization of these cytoskeleton markers. Our further investigation reveals a mechanism by which cell attachment induces uropod pMLC polarization (Figure S7G). Namely, increased local PM curvature resulting from cell contact to a surface recruits an F-BAR-domain-containing protein SRGAP2, which in turn activates a lipid kinase PI4KA, resulting in PM PtdIns4P polarization. PM PtdIns4P is recognized by RPH3A, an effector of RAB21, leading to polarization of RAB21, PIP5K1C90, and eventually pMLC. Thus, cell contact to a surface or PM curvature change alone can induce some forms of neutrophil polarization, namely SRGAP2 and PM PtdIns4P polarization, independent of chemokine or integrin signaling. However, subsequent polarization of RPH3A, RAB21, PIP5K1C90, and pMLC, as depicted in Figure S7G, requires both PM curvature change and chemokine and/or integrin stimulation (Yuan et al., 2017; Tang et al., 2011; Xu et al., 2010).

We show that $CD8^+$ T cells also require PM curvature change for their cytoskeleton polarization. Thus, our findings on cell polarization initiation likely extend beyond neutrophils to other circulating leukocytes. In addition to alteration in PM curvature through cell attachment and pipette pulling described in this study, other forms of cell shape changes including cells squeezing through matrices in 3D migration can also presumably lead to cell polarization through similar mechanisms. Moreover, our findings suggest that caution is warranted for the interpretation of many of the previous observations made with attached cells, as these cells already possess certain forms of polarization that could instruct polarization events controlled by extracellular chemical stimuli and might not have been fully considered in the interpretation of the results. This is particularly true for the interpretation of cell polarization under uniform extracellular chemical stimulation and "spontaneous" polarization. PM curvature-induced cellular polarity unraveled in this study may have unmasked the mystery of "stochastic polarity" that was proposed to be needed for these types of cellular polarization (Ladoux et al., 2016; Woodham and Machesky, 2014; Asnacios and Hamant, 2012; Altschuler et al., 2008; Sohrmann and Peter, 2003).

SRGAP2 and its F-BAR domain were shown to recognize concave membrane curvature (Sporny et al., 2017; Charrier et al., 2012; Guerrier et al., 2009). This is consistent with our observation of recruitment of SRGAP2 to the cusps above the coverslip (dorsoventral polarization) when cells were placed on a coverslip (Figure 6B) because of increases in PM curvature at the cusps. This cell-contact-induced dorsoventral SRGAP2 polarization may represent the initial step of breaking cellular symmetry. The anteroposterior polarization of FBAR-GFP (Figures 6C and 6D) is the consequence of lateral cell movement during cell settlement in the static experiments or under shear flow. The lateral movement presumably results in a steeper curvature at the trailing end of the cell, leading to increased localization of SRGAP2 via its F-BAR domain. This idea is well supported by the significant positive correlation of steeper PM curvature with greater localization of SRGAP2 FBAR-GFP (Figure S6F) and PtdIns4P probe GFP-P4M (Figure S7D) revealed by the single neutrophil aspiration experiments. Because shear flow is a physiological norm for neutrophils, anteroposterior polarization of SRGAP2 and its downstream events would unsurprisingly occur at a high rate *in vivo*. Indeed, FBAR-GFP was observed in inflamed blood vessels *in vivo* under flow in live zebrafish (Figure 6F).

We showed that PI4KA was required for cell attachment-induced PM PtdIns4P polarization. The stimulation of PI4KA kinase activity by SRGAP2 provides a mechanism for SRGAP2 polarization to lead to PtdIns4P polarization. Although there might be other mechanisms, PI4KA polarization unlikely is one of them, as we could not observe polarization of endogenous or tagged PI4KA by immunostaining or PI4KA-GFP in live cells under the manipulations that caused polarization of SRGAP2 and PtdIns4P (data not shown).

While we have characterized a detailed biochemical mechanism for cell attachment or membrane curvature to regulate "back" polarization of PIP5K1C90 and pMLC, how cell attachment dictates "front" F-actin polarization in response to chemical stimulation remains unknown. We assume that PM curvature changes and proteins that recognize the curvature or cell shape changes may be involved. However, none of the BAR-domain-containing proteins that we believe are expressed in neutrophils

(F) GFP-P4M polarization does not depend on chemical stimulation. Neutrophils were transfected with GFP-P4M and treated as in Figure 6G. Cells attached to PK-coated coverslips were imaged by confocal microscopy. Cells showing anteroposterior polarization were scored. Each data point represents the average of more than 10 cells per observation field.

(G) Higher membrane curvature generated by micropipette aspiration leads to polarization of GFP-P4M. MemRed expressing neutrophils from mT/mG mice were transfected with GFP-P4M. The bright spots are likely Golgi. Images of a representative cell are shown. The experiments were repeated ten times. Scale bar in (G) is 3 μm, and the grid scale in (A)–(D) is 1 μm.

See also Figure S7.

were involved (Figure S2A). It is possible that there is a broader functional redundancy or different types of proteins that recognize the membrane curvature and/or cell shape change are required for the F-actin polarization. Future work is warranted to investigate these questions.

STAR★METHODS

Detailed methods are provided in the online version of this paper and include the following:

- KEY RESOURCES TABLE
- CONTACT FOR REAGENT AND RESOURCE SHARING
- EXPERIMENTAL MODEL AND SUBJECT DETAILS
  - Mice
  - Zebrafish
  - Cell Lines
- METHOD DETAILS
  - Neutrophil Preparation and Transfection
  - Immunostaining and Observation of Neutrophils
  - Flow Chamber Assay
  - ICAM-binding Assay
  - Integrin Blocking and Neutrophil Spreading
  - In Vitro Chemotaxis Assay in a Dunn Chamber
  - Intravital Microscopy
  - Echocardiography
  - Murine Heart Ischemia/reperfusion (IR) Models
  - Blood Cell Counts
  - Immunoprecipitation
  - Preparation of Recombinant Proteins
  - Buoyant Density Flotation of Liposome Assay
  - PI4KA Lipid Kinase Assay
  - $CD8^+$ T cells Preparation and Transfection
  - $CD8^+$ T cells Immunostaining
  - Micropipette Aspiration Assay
- QUANTIFICATION AND STATISTICAL ANALYSIS

SUPPLEMENTAL INFORMATION

Supplemental Information can be found online at https://doi.org/10.1016/j.devcel.2019.02.023.

ACKNOWLEDGMENTS

We thank Michelle Orsulak for technical assistance, Pietro De Camilli for providing PIP5K1C antibody (Di Paolo et al., 2002) and human PI4KA cDNA, Guangxin Li and George Tellides for the mT/mG mice, Felix Rivera-Molina and Derek K. Toomre for assistance with spinning disk microscopy, and Elias Lolis for the MIP2 proteins (Rajasekaran et al., 2012). The work is supported by National Institutes of Health grants to D.W. (R35HL135805), W.T. (R01HL145152), E.K. (R01GM108954 and R01GM114513), Z.S. (R01HL125885), and F.P. (R01NSNS067557) and the Snyder Mouse Phenomics Resources Laboratory and Live Cell Imaging Facility, both of which were funded by the Snyder Institute for Chronic Diseases at the University of Calgary, Calgary, Canada.

AUTHOR CONTRIBUTIONS

D.W., W.T., and E.K. supervised the project and developed the concepts. C.R., Q.Y., M.B., X.Z., B.P., J.Z., D.K., J.G.-H., and W.X. performed the experiments and analyzed the data. D.W., W.T., E.K., C.R., Q.Y., M.B., D.K., R.F., B.P., P.K., W.P., Z.S., Y.O., and F.P. designed the experiments and wrote the paper. All authors were involved in the writing and final approval of the manuscript.

DECLARATION OF INTERESTS

The authors declare no competing interests.

Received: March 15, 2018
Revised: January 15, 2019
Accepted: February 25, 2019
Published: March 28, 2019

REFERENCES

Altschuler, S.J., Angenent, S.B., Wang, Y., and Wu, L.F. (2008). On the spontaneous emergence of cell polarity. Nature *454*, 886–889.

Asnacios, A., and Hamant, O. (2012). The mechanics behind cell polarity. Trends Cell Biol. *22*, 584–591.

Basit, A., Tang, W., and Wu, D. (2016). shRNA-induced gene knockdown in vivo to investigate neutrophil function. Methods Mol. Biol. *1407*, 169–177.

Baskin, J.M., Wu, X., Christiano, R., Oh, M.S., Schauder, C.M., Gazzerro, E., Messa, M., Baldassari, S., Assereto, S., Biancheri, R., et al. (2016). The leukodystrophy protein FAM126A (hyccin) regulates PtdIns(4)P synthesis at the plasma membrane. Nat. Cell Biol. *18*, 132–138.

Bodin, S., and Welch, M.D. (2005). Plasma membrane organization is essential for balancing competing pseudopod- and uropod-promoting signals during neutrophil polarization and migration. Mol. Biol. Cell *16*, 5773–5783.

Boswell, K.L., James, D.J., Esquibel, J.M., Bruinsma, S., Shirakawa, R., Horiuchi, H., and Martin, T.F. (2012). Munc13-4 reconstitutes calcium-dependent SNARE-mediated membrane fusion. J. Cell Biol. *197*, 301–312.

Brombacher, E., Urwyler, S., Ragaz, C., Weber, S.S., Kami, K., Overduin, M., and Hilbi, H. (2009). Rab1 guanine nucleotide exchange factor SidM is a major phosphatidylinositol 4-phosphate-binding effector protein of Legionella pneumophila. J. Biol. Chem. *284*, 4846–4856.

Charrier, C., Joshi, K., Coutinho-Budd, J., Kim, J.E., Lambert, N., de Marchena, J., Jin, W.L., Vanderhaeghen, P., Ghosh, A., Sassa, T., et al. (2012). Inhibition of SRGAP2 function by its human-specific paralogs induces neoteny during spine maturation. Cell *149*, 923–935.

Christofidou-Solomidou, M., Nakada, M.T., Williams, J., Muller, W.A., and DeLisser, H.M. (1997). Neutrophil platelet endothelial cell adhesion molecule-1 participates in neutrophil recruitment at inflammatory sites and is down-regulated after leukocyte extravasation. J. Immunol. *158*, 4872–4878.

Clarke, J.H., Richardson, J.P., Hinchliffe, K.A., and Irvine, R.F. (2007). Type II PtdInsP kinases: location, regulation and function. Biochem. Soc. Symp. 149–159.

Corbalan-Garcia, S., and Gómez-Fernández, J.C. (2014). Signaling through C2 domains: more than one lipid target. Biochim. Biophys. Acta *1838*, 1536–1547.

Coutinho-Budd, J., Ghukasyan, V., Zylka, M.J., and Polleux, F. (2012). The F-BAR domains from srGAP1, srGAP2 and srGAP3 regulate membrane deformation differently. J. Cell Sci. *125*, 3390–3401.

Cramer, L.P. (2010). Forming the cell rear first: breaking cell symmetry to trigger directed cell migration. Nat. Cell Biol. *12*, 628–632.

De Matteis, M.A., Wilson, C., and D'Angelo, G. (2013). Phosphatidylinositol-4-phosphate: the Golgi and beyond. Bioessays *35*, 612–622.

de Oliveira, S., Rosowski, E.E., and Huttenlocher, A. (2016). Neutrophil migration in infection and wound repair: going forward in reverse. Nat. Rev. Immunol. *16*, 378–391.

Devreotes, P., and Horwitz, A.R. (2015). Signaling networks that regulate cell migration. Cold Spring Harb. Perspect. Biol. *7*, a005959.

Di Paolo, G., Pellegrini, L., Letinic, K., Cestra, G., Zoncu, R., Voronov, S., Chang, S., Guo, J., Wenk, M.R., and De Camilli, P. (2002). Recruitment and regulation of phosphatidylinositol phosphate kinase type 1 gamma by the FERM domain of talin. Nature *420*, 85–89.

Francis, S.A., Shen, X., Young, J.B., Kaul, P., and Lerner, D.J. (2006). Rho GEF Lsc is required for normal polarization, migration, and adhesion of formyl-peptide-stimulated neutrophils. Blood *107*, 1627–1635.

Frost, A., Unger, V.M., and De Camilli, P. (2009). The BAR domain superfamily: membrane-molding macromolecules. Cell *137*, 191–196.

Gao, K., Tang, W., Li, Y., Zhang, P., Wang, D., Yu, L., Wang, C., and Wu, D. (2015). Front-signal-dependent accumulation of the RHOA inhibitor FAM65B at leading edges polarizes neutrophils. J. Cell Sci. *128*, 992–1000.

Gómez-Moutón, C., and Mañes, S. (2007). Establishment and maintenance of cell polarity during leukocyte chemotaxis. Cell Adh. Migr. *1*, 69–76.

Graziano, B.R., and Weiner, O.D. (2014). Self-organization of protrusions and polarity during eukaryotic chemotaxis. Curr. Opin. Cell Biol. *30*, 60–67.

Guerrier, S., Coutinho-Budd, J., Sassa, T., Gresset, A., Jordan, N.V., Chen, K., Jin, W.L., Frost, A., and Polleux, F. (2009). The F-BAR domain of srGAP2 induces membrane protrusions required for neuronal migration and morphogenesis. Cell *138*, 990–1004.

Hall, C., Flores, M.V., Storm, T., Crosier, K., and Crosier, P. (2007). The zebrafish lysozyme C promoter drives myeloid-specific expression in transgenic fish. BMC Dev. Biol. *7*, 42.

Hammond, G.R., Fischer, M.J., Anderson, K.E., Holdich, J., Koteci, A., Balla, T., and Irvine, R.F. (2012). PI4P and PI(4,5)P2 are essential but independent lipid determinants of membrane identity. Science *337*, 727–730.

Hammond, G.R., Machner, M.P., and Balla, T. (2014). A novel probe for phosphatidylinositol 4-phosphate reveals multiple pools beyond the Golgi. J. Cell Biol. *205*, 113–126.

Hammond, G.R., Schiavo, G., and Irvine, R.F. (2009). Immunocytochemical techniques reveal multiple, distinct cellular pools of PtdIns4P and PtdIns(4,5)P(2). Biochem. J. *422*, 23–35.

Hind, L.E., Vincent, W.J., and Huttenlocher, A. (2016). Leading from the back: the role of the uropod in neutrophil polarization and migration. Dev. Cell *38*, 161–169.

Hoyer, F.F., and Nahrendorf, M. (2017). Neutrophil contributions to ischaemic heart disease. Eur. Heart J. *38*, 465–472.

Insall, R.H. (2010). Understanding eukaryotic chemotaxis: a pseudopod-centred view. Nat. Rev. Mol. Cell Biol. *11*, 453–458.

Jethwa, N., Fili, N., and Larijani, B. (2012). Acute depletion of plasma membrane phospholipids-dissecting the roles of PtdIns(4)P and PtdIns(4,5)P2. J. Chem. Biol. *5*, 137–139.

Kolaczkowska, E., and Kubes, P. (2013). Neutrophil recruitment and function in health and inflammation. Nat. Rev. Immunol. *13*, 159–175.

Konstandin, M.H., Sester, U., Klemke, M., Weschenfelder, T., Wabnitz, G.H., and Samstag, Y. (2006). A novel flow-cytometry-based assay for quantification of affinity and avidity changes of integrins. J. Immunol. Methods *310*, 67–77.

Kumar, S., Xu, J., Perkins, C., Guo, F., Snapper, S., Finkelman, F.D., Zheng, Y., and Filippi, M.D. (2012). Cdc42 regulates neutrophil migration via crosstalk between WASp, CD11b, and microtubules. Blood *120*, 3563–3574.

Kwon, Y., Hofmann, T., and Montell, C. (2007). Integration of phosphoinositide- and calmodulin-mediated regulation of TRPC6. Mol. Cell *25*, 491–503.

Ladoux, B., Mège, R.M., and Trepat, X. (2016). Front-rear polarization by mechanical cues: From single cells to tissues. Trends Cell Biol. *26*, 420–433.

Lam, P.Y., Fischer, R.S., Shin, W.D., Waterman, C.M., and Huttenlocher, A. (2014). Spinning disk confocal imaging of neutrophil migration in zebrafish. Methods Mol. Biol. *1124*, 219–233.

Ley, K., Laudanna, C., Cybulsky, M.I., and Nourshargh, S. (2007). Getting to the site of inflammation: the leukocyte adhesion cascade updated. Nat. Rev. Immunol. *7*, 678–689.

Liu, L., Cara, D.C., Kaur, J., Raharjo, E., Mullaly, S.C., Jongstra-Bilen, J., Jongstra, J., and Kubes, P. (2005). LSP1 is an endothelial gatekeeper of leukocyte transendothelial migration. J. Exp. Med. *201*, 409–418.

Liu, L., Das, S., Losert, W., and Parent, C.A. (2010). mTORC2 regulates neutrophil chemotaxis in a cAMP- and RhoA-dependent fashion. Dev. Cell *19*, 845–857.

Loison, F., Zhu, H., Karatepe, K., Kasorn, A., Liu, P., Ye, K., Zhou, J., Cao, S., Gong, H., Jenne, D.E., et al. (2014). Proteinase 3-dependent caspase-3 cleavage modulates neutrophil death and inflammation. J. Clin. Invest. *124*, 4445–4458.

Majumdar, R., Sixt, M., and Parent, C.A. (2014). New paradigms in the establishment and maintenance of gradients during directed cell migration. Curr. Opin. Cell Biol. *30*, 33–40.

Muzumdar, M.D., Tasic, B., Miyamichi, K., Li, L., and Luo, L. (2007). A global double-fluorescent Cre reporter mouse. Genesis *45*, 593–605.

Nakatsu, F., Baskin, J.M., Chung, J., Tanner, L.B., Shui, G., Lee, S.Y., Pirruccello, M., Hao, M., Ingolia, N.T., Wenk, M.R., et al. (2012). PtdIns4P synthesis by PI4KIIIalpha at the plasma membrane and its impact on plasma membrane identity. J. Cell Biol. *199*, 1003–1016.

Navaroli, D.M., Bellvé, K.D., Standley, C., Lifshitz, L.M., Cardia, J., Lambright, D., Leonard, D., Fogarty, K.E., and Corvera, S. (2012). Rabenosyn-5 defines the fate of the transferrin receptor following clathrin-mediated endocytosis. Proc. Natl. Acad. Sci. USA *109*, E471–E480.

Nichols, J.M., Veltman, D., and Kay, R.R. (2015). Chemotaxis of a model organism: progress with Dictyostelium. Curr. Opin. Cell Biol. *36*, 7–12.

Nourshargh, S., and Alon, R. (2014). Leukocyte migration into inflamed tissues. Immunity *41*, 694–707.

Rajasekaran, D., Keeler, C., Syed, M.A., Jones, M.C., Harrison, J.K., Wu, D., Bhandari, V., Hodsdon, M.E., and Lolis, E.J. (2012). A model of GAG/MIP-2/CXCR2 interfaces and its functional effects. Biochemistry *51*, 5642–5654.

Record, J., Malinova, D., Zenner, H.L., Plagnol, V., Nowak, K., Syed, F., Bouma, G., Curtis, J., Gilmour, K., Cale, C., et al. (2015). Immunodeficiency and severe susceptibility to bacterial infection associated with a loss-of-function homozygous mutation of MKL1. Blood *126*, 1527–1535.

Ridley, A.J., Schwartz, M.A., Burridge, K., Firtel, R.A., Ginsberg, M.H., Borisy, G., Parsons, J.T., and Horwitz, A.R. (2003). Cell migration: integrating signals from front to back. Science *302*, 1704–1709.

Rizo, J., and Südhof, T.C. (1998). C2-domains, structure and function of a universal Ca2+-binding domain. J. Biol. Chem. *273*, 15879–15882.

Sánchez-Madrid, F., and Serrador, J.M. (2009). Bringing up the rear: defining the roles of the uropod. Nat. Rev. Mol. Cell Biol. *10*, 353–359.

Schoebel, S., Blankenfeldt, W., Goody, R.S., and Itzen, A. (2010). High-affinity binding of phosphatidylinositol 4-phosphate by Legionella pneumophila DrrA. EMBO Rep. *11*, 598–604.

Seveau, S., Eddy, R.J., Maxfield, F.R., and Pierini, L.M. (2001). Cytoskeleton-dependent membrane domain segregation during neutrophil polarization. Mol. Biol. Cell *12*, 3550–3562.

Shi, Y., Zhang, J., Mullin, M., Dong, B., Alberts, A.S., and Siminovitch, K.A. (2009). The mDial formin is required for neutrophil polarization, migration, and activation of the LARG/RhoA/ROCK signaling axis during chemotaxis. J. Immunol. *182*, 3837–3845.

Shin, M.E., He, Y., Li, D., Na, S., Chowdhury, F., Poh, Y.C., Collin, O., Su, P., de Lanerolle, P., Schwartz, M.A., et al. (2010). Spatiotemporal organization, regulation, and functions of tractions during neutrophil chemotaxis. Blood *116*, 3297–3310.

Simunovic, M., Voth, G.A., Callan-Jones, A., and Bassereau, P. (2015). When physics takes Over: BAR proteins and membrane curvature. Trends Cell Biol. *25*, 780–792.

Sohrmann, M., and Peter, M. (2003). Polarizing without a c(l)ue. Trends Cell Biol. *13*, 526–533.

Sporny, M., Guez-Haddad, J., Kreusch, A., Shakartzi, S., Neznansky, A., Cross, A., Isupov, M.N., Qualmann, B., Kessels, M.M., and Opatowsky, Y. (2017). Structural history of human SRGAP2 proteins. Mol. Biol. Evol. *34*, 1463–1478.

Srinivasan, S., Wang, F., Glavas, S., Ott, A., Hofmann, F., Aktories, K., Kalman, D., and Bourne, H.R. (2003). Rac and Cdc42 play distinct roles in regulating PI(3,4,5)P3 and polarity during neutrophil chemotaxis. J. Cell Biol. *160*, 375–385.

Stachowiak, M.R., Laplante, C., Chin, H.F., Guirao, B., Karatekin, E., Pollard, T.D., and O'Shaughnessy, B. (2014). Mechanism of cytokinetic contractile ring constriction in fission yeast. Dev. Cell *29*, 547–561.

Subramanian, K.K., Jia, Y., Zhu, D., Simms, B.T., Jo, H., Hattori, H., You, J., Mizgerd, J.P., and Luo, H.R. (2007). Tumor suppressor PTEN is a physiologic

suppressor of chemoattractant-mediated neutrophil functions. Blood *109*, 4028–4037.

Suetsugu, S., Toyooka, K., and Senju, Y. (2010). Subcellular membrane curvature mediated by the BAR domain superfamily proteins. Semin. Cell Dev. Biol. *21*, 340–349.

Sun, C.X., Magalhães, M.A., and Glogauer, M. (2007). Rac1 and Rac2 differentially regulate actin free barbed end formation downstream of the fMLP receptor. J. Cell Biol. *179*, 239–245.

Tang, W., Zhang, Y., Xu, W., Harden, T.K., Sondek, J., Sun, L., Li, L., and Wu, D. (2011). A PLCβ/PI3Kγ-GSK3 signaling pathway regulates cofilin phosphatase slingshot2 and neutrophil polarization and chemotaxis. Dev. Cell *21*, 1038–1050.

Tasaka, S., Qin, L., Saijo, A., Albelda, S.M., DeLisser, H.M., and Doerschuk, C.M. (2003). Platelet endothelial cell adhesion molecule-1 in neutrophil emigration during acute bacterial pneumonia in mice and rats. Am. J. Respir. Crit. Care Med. *167*, 164–170.

Van Keymeulen, A., Wong, K., Knight, Z.A., Govaerts, C., Hahn, K.M., Shokat, K.M., and Bourne, H.R. (2006). To stabilize neutrophil polarity, PIP3 and Cdc42 augment RhoA activity at the back as well as signals at the front. J. Cell Biol. *174*, 437–445.

Vinten-Johansen, J. (2004). Involvement of neutrophils in the pathogenesis of lethal myocardial reperfusion injury. Cardiovasc. Res. *61*, 481–497.

Wang, F. (2009). The signaling mechanisms underlying cell polarity and chemotaxis. Cold Spring Harb. Perspect. Biol. *1*, a002980.

Wang, X., Ha, T., Zou, J., Ren, D., Liu, L., Zhang, X., Kalbfleisch, J., Gao, X., Williams, D., and Li, C. (2014). MicroRNA-125b protects against myocardial ischaemia/reperfusion injury via targeting p53-mediated apoptotic signalling and TRAF6. Cardiovasc. Res. *102*, 385–395.

Wang, Z., Liu, B., Wang, P., Dong, X., Fernandez-Hernando, C., Li, Z., Hla, T., Li, Z., Claffey, K., Smith, J.D., et al. (2008). Phospholipase C beta3 deficiency leads to macrophage hypersensitivity to apoptotic induction and reduction of atherosclerosis in mice. J. Clin. Invest. *118*, 195–204.

Wasilewski, M.A., Grisanti, L.A., Song, J., Carter, R.L., Repas, A.A., Myers, V.D., Gao, E., Koch, W.J., Cheung, J.Y., Feldman, A.M., et al. (2016). Vasopressin type 1A receptor deletion enhances cardiac contractility, β-adrenergic receptor sensitivity and acute cardiac injury-induced dysfunction. Clin. Sci. (Lond) *130*, 2017–2027.

Wong, K., Van Keymeulen, A., and Bourne, H.R. (2007). PDZRhoGEF and myosin II localize RhoA activity to the back of polarizing neutrophil-like cells. J. Cell Biol. *179*, 1141–1148.

Woodham, E.F., and Machesky, L.M. (2014). Polarised cell migration: intrinsic and extrinsic drivers. Curr. Opin. Cell Biol. *30*, 25–32.

Xu, J., Wang, F., Van Keymeulen, A., Herzmark, P., Straight, A., Kelly, K., Takuwa, Y., Sugimoto, N., Mitchison, T., and Bourne, H.R. (2003). Divergent signals and cytoskeletal assemblies regulate self-organizing polarity in neutrophils. Cell *114*, 201–214.

Xu, J., Wang, F., Van Keymeulen, A., Rentel, M., and Bourne, H.R. (2005). Neutrophil microtubules suppress polarity and enhance directional migration. Proc. Natl. Acad. Sci. USA *102*, 6884–6889.

Xu, W., Wang, P., Petri, B., Zhang, Y., Tang, W., Sun, L., Kress, H., Mann, T., Shi, Y., Kubes, P., et al. (2010). Integrin-induced PIP5K1C kinase polarization regulates neutrophil polarization, directionality, and in vivo infiltration. Immunity *33*, 340–350.

Xu, X., and Jin, T. (2015). The novel functions of the PLC/PKC/PKD signaling axis in G protein-coupled receptor-mediated chemotaxis of neutrophils. J. Immunol. Res. *2015*, 1–10.

Yoo, S.K., Deng, Q., Cavnar, P.J., Wu, Y.I., Hahn, K.M., and Huttenlocher, A. (2010). Differential regulation of protrusion and polarity by PI3K during neutrophil motility in live zebrafish. Dev. Cell *18*, 226–236.

Yu, J.A., Castranova, D., Pham, V.N., and Weinstein, B.M. (2015). Single-cell analysis of endothelial morphogenesis in vivo. Development *142*, 2951–2961.

Yuan, Q., Ren, C., Xu, W., Petri, B., Zhang, J., Zhang, Y., Kubes, P., Wu, D., and Tang, W. (2017). PKN1 directs polarized RAB21 vesicle trafficking via RPH3A and is important for neutrophil adhesion and ischemia-reperfusion injury. Cell Rep. *19*, 2586–2597.

Zhang, Y., Bai, X.T., Zhu, K.Y., Jin, Y., Deng, M., Le, H.Y., Fu, Y.F., Chen, Y., Zhu, J., Look, A.T., et al. (2008). In vivo interstitial migration of primitive macrophages mediated by JNK-matrix metalloproteinase 13 signaling in response to acute injury. J. Immunol. *181*, 2155–2164.

Zhang, Y., Tang, W., Jones, M.C., Xu, W., Halene, S., and Wu, D. (2010). Different roles of G protein subunits beta1 and beta2 in neutrophil function revealed by gene expression silencing in primary mouse neutrophils. J. Biol. Chem. *285*, 24805–24814.

Zhang, Y., Tang, W., Zhang, H., Niu, X., Xu, Y., Zhang, J., Gao, K., Pan, W., Boggon, T.J., Toomre, D., et al. (2013). A network of interactions enables CCM3 and STK24 to coordinate UNC13D-driven vesicle exocytosis in neutrophils. Dev. Cell *27*, 215–226.

Please cite this article in press as: Ren et al., Leukocyte Cytoskeleton Polarization Is Initiated by Plasma Membrane Curvature from Cell Attachment, Developmental Cell (2019), https://doi.org/10.1016/j.devcel.2019.02.023

STAR★METHODS

KEY RESOURCES TABLE

REAGENT or RESOURCE	SOURCE	IDENTIFIER
Antibodies		
Mouse monoclonal anti-Phospho-Myosin Light Chain 2	Cell Signaling Technology	Cat#3675; RRID: AB_2250969
Rabbit polyclonal anti-Phospho-Myosin Light Chain 2	Cell Signaling Technology	Cat# 3671; RRID: AB_330248
Goat polyclonal anti-SRGAP2 (C14)	Santa Cruz Biotechnology	Cat# sc-103497; RRID: AB_2270918
Mouse monoclonal anti-SRGAP2 (G10)	Santa Cruz Biotechnology	Cat# sc-398399
Mouse monoclonal anti-PtdIns(4)P	Echelon Biosciences	Cat# Z-P004; RRID: AB_11127796
Rabbit polyclonal anti-TGN38	Novus Biologicals	Cat# NBP1-03495; RRID: AB_1522533
Rabbit monoclonal anti-Phospho-Akt (Ser473)	Cell Signaling Technology	Cat# 4060; RRID: AB_2315049
Rat monoclonal anti-Ly6G	BD Biosciences	Cat# 560603; RRID: AB_1727564
Rat monoclonal anti-Ly-6B.2	Thermo Fisher Scientific	Cat# MA5-16539; RRID: AB_2538044
Mouse monoclonal anti-His-Tag	Cell Signaling Technology	Cat# 2366; RRID: AB_2115719
Mouse monoclonal anti-HA.11	Covance Research Products	Cat# MMS-101R-1000; RRID: AB_291262
Rabbit polyclonal anti-RAB21	Sigma-Aldrich	Cat# R4405; RRID:AB_1841130
Rabbit polyclonal anti-RPH3A	Aviva Systems Biology	Cat# ARP59498_P050; RRID: AB_10875309
Hamster monoclonal anti-CD29	Thermo Fisher Scientific	Cat# 16-0291-85; RRID: AB_657731
Rat monoclonal anti-CD18	BD Biosciences	Cat# 555280; RRID: AB_395703
Rat monoclonal anti-CD11b APC	Thermo Fisher Scientific	Cat# 17-0112-81; RRID: AB_469342
Hamster monoclonal anti-CD3e	Thermo Fisher Scientific	Cat# 16-0031-81; RRID: AB_468846
Hamster monoclonal anti-CD28	Thermo Fisher Scientific	Cat# 16-0281-81; RRID: AB_468920
Rabbit monoclonal anti-Beta-Actin	Cell Signaling Technology	Cat# 4970; RRID: AB_2223172
Rabbit polyclonal anti-Beta-Tubulin	Cell Signaling Technology	Cat# 2146; RID: AB_2210545
Rabbit polyclonal anti-PIP5K1C90	Di Paolo et al., (2002)	N/A
Rat monoclonal anti-Ly-6G/Ly-6C(Gr-1) conjugated to PE	Thermo Fisher Scientific	Cat# 50-109-94
Rat monoclonal anti-CD31/PECAM-1 Alexa Fluor® 647-conjugated	Thermo Fisher Scientific	Cat# A14716
Bacterial and Virus Strains		
E. coli BL21(DE3)	New England Biolabs	Cat# C2527I
Chemicals, Peptides, and Recombinant Proteins		
Alexa Fluor™ 633 Phalloidin	Thermo Fisher Scientific	Cat# A22284
Rapamycin	Millipore Sigma	Cat# 553210
Pertussis Toxin	Thermo Fisher Scientific	Cat# PHZ1174
Protein A/G PLUS-Agarose	Santa Cruz Biotechnology	Cat# sc-2003
CyGEL™	Abcam	Cat# ab109204
CellTrace™ CFSE	Thermo Fisher Scientific	Cat# C34554
CellTrace™ Far Red	Thermo Fisher Scientific	Cat# C34564
Alexa Fluor® 647 AffiniPure F(ab')$_2$ Fragment Goat Anti-Human IgG, Fcγ Fragment Specific	Jackson Immunoresearch	Cat# 109-606-098
Ni-NTA agarose beads	GE Healthcare	Cat# 17531801
Phosphatidylinositol 3-phosphate diC16 (PI(3)P diC16)	Echelon Biosciences	Cat# P-3016
Phosphatidylinositol 3,4-bisphosphate diC16 (PI(3,4)P2 diC16)	Echelon Biosciences	Cat# P-3416
Phosphatidylinositol 3,5-bisphosphate diC16 (PI(3,5)P2 diC16)	Echelon Biosciences	Cat# P-3516
Phosphatidylinositol 3,4,5-trisphosphate diC16 (PI(3,4,5)P3 diC16)	Echelon Biosciences	Cat# P-3916
Phosphatidylinositol 4-phosphate diC16 (PI(4)P diC16)	Echelon Biosciences	Cat# P-4016

(*Continued on next page*)

Continued

REAGENT or RESOURCE	SOURCE	IDENTIFIER
Phosphatidylinositol 4,5-bisphosphate diC16 (PI(4,5)P2 diC16)	Echelon Biosciences	Cat# P-4516
Phosphatidylinositol 5-phosphate diC16 (PI(5)P diC16)	Echelon Biosciences	Cat# P-5016
Phosphocholine (PC)	Avanti Polar Lipids	Cat# 850457C
Phosphatidylserine (PS)	Avanti Polar Lipids	Cat# 840035C
N-Formyl-Met-Leu-Phe (fMLP)	Sigma-Aldrich	Cat# 47729
Recombinant Mouse ICAM-1/CD54 Fc Chimera Protein, CF	R&D Systems	Cat# 796-IC-050
Recombinant Mouse CXCL12/SDF-1 alpha Protein	Novus Biologicals	Cat# NBP2-35155
Recombinant Murine GM-CSF	PeproTech	Cat# 315-03
Recombinant Murine TNF-α	PeproTech	Cat# 315-01A
Murine MIP2	Rajasekaran et al. (2012)	N/A
Critical Commercial Assays		
Human monocyte nucleofection kit	Lonza	Cat# VPA-1007
CD8a+ T Cell Isolation Kit, mouse	Miltenyi Biotec	Cat# 130-104-075
Mouse T Cell NucleofectorTM Kit	Lonza	Cat# VPA-1006
Experimental Models: Cell Lines		
Mouse endothelial cells	Wang et al. (2008)	N/A
HEK293T cells	ATCC	ATCC® CRL-3216™
Experimental Models: Organisms/Strains		
Mouse: *SRGAP2^{Gt}(XH102)$^{Byg/Mmcd}$*	Charrier et al. (2012)	N/A
Mouse: B6;129P2-*Rph3a^{tm1Sud}*/J	The Jackson Laboratory	JAX: 006374
Mouse: *mT/mG*	Muzumdar et al. (2007)	N/A
Zebrafish: *Tg(kdrl:mRFP)*	Yu et al. (2015)	N/A
Zebrafish: *Tg(lyz:FBAR-GFP)*	This paper	N/A
Oligonucleotides		
Control siRNA	Thermo Fisher Scientific	Cat# AM4611
SiRNA: Fnbp1	Dharmacon	Cat# L-062539-01-0005
SiRNA: Arhgap17	Dharmacon	Cat# L-040551-02-0005
SiRNA: Sh3bp1	Dharmacon	Cat# L-044982-01-0005
SiRNA: Fes	Dharmacon	Cat# L-043381-00-0005
SiRNA: Srgap2	Dharmacon	Cat# L-040298-01-0005
SiRNA: Arhgap4	Dharmacon	Cat# L-054858-01-0005
SiRNA: Pi4ka	Dharmacon	Cat# L-066305-00-0005
SiRNA: Pi4kb	Dharmacon	Cat# L-056390-00-0005
SiRNA: Pi4k2a	Dharmacon	Cat# L-065311-00-0005
SiRNA: Pi4k2b	Dharmacon	Cat# L-065308-00-0005
Recombinant DNA		
cDNA mouse SRGAP2	Dharmacon	Cat# MMM1013-202710387
cDNA mouse RPH3A	Dharmacon	Cat# MMM1013-202769795
cDNA mouse PI4KA	Dharmacon	Cat# MMM1013-202859892
cDNA human PI4KA	Nakatsu et al. (2012)	N/A
Plasmid: TagRFP-T-EEA1	Navaroli et al. (2012)	Addgene Plasmid #42635
Plasmid: pcDNA3-AKT-PH-GFP	Kwon et al. (2007)	Addgene Plasmid # 18836
Plasmid: GFP-P4M-SidM	Hammond et al. (2014)	Addgene Plasmid # 51469
Plasmid: Lyn11-FRB-mcherry	Hammond et al. (2012)	Addgene Plasmid # 38004
Plasmid: PJ-INPP5E	Hammond et al. (2012)	Addgene Plasmid # 38001
Plasmid: PJ-Sac	Hammond et al. (2012)	Addgene Plasmid # 38000
Plasmid: tol2-mpx-mCherry	Yoo et al. (2010)	Addgene Plasmid # 29585

(*Continued on next page*)

Continued

REAGENT or RESOURCE	SOURCE	IDENTIFIER
Plasmid: pAAV-FBAR-GFP	This paper	N/A
Plasmid: pAAV-GFP-P4M	This paper	N/A
Plasmid: pAAV-SRGAP2-HA	This paper	N/A
Plasmid: pAAV-SRGAP2(R527L)-HA	This paper	N/A
Plasmid: pAAV-SRGAP2(ΔF-BAR)-HA	This paper	N/A
Plasmid: pAAV-PI4KA(human)-HA	This paper	N/A
Plasmid: pAAV-PI4KA(mouse)-Myc	This paper	N/A
Plasmid: pAAV-FBAR-TagRFP	This paper	N/A
Plasmid: tol2-lyz-FBAR-GFP	This paper	N/A
Software and Algorithms		
Image J. (v1.48K)	NIH	http://imagej.nih.gov/ij/
Leica Application Suite	Leica Biosystems	https://www.leica-microsystems.com/
Volocity 6.3	Perkin-Elmer	http://www.perkinelmer.com/
Imaris 7.2.3	Bitplane	http://www.bitplane.com/
MetaMorph	Molecular Devices	https://www.moleculardevices.com/

CONTACT FOR REAGENT AND RESOURCE SHARING

Further information and requests for resources and reagents should be directed to and will be fulfilled by the Lead Contact, Dianqing Wu (dan.wu@yale.edu).

EXPERIMENTAL MODEL AND SUBJECT DETAILS

Mice

The SRGAP2-null mice (*SRGAP2*^{Gt}*(XH102)*$^{Byg/Mmcd}$) were described previously (Charrier et al., 2012). The RPH3A-null mice (B6;129P2-*Rph3a*^{tm1Sud}/J) were obtained from the Jackson Lab. The *mT/mG* mice, a double-fluorescent Cre reporter mouse that expresses membrane-targeted tandem dimer Tomato (mT) prior to Cre-mediated excision were kindly provided by Dr. Guangxin Li and Dr. George Tellides (Muzumdar et al., 2007). Wildtype C57BL mice were purchased from Jackson Lab. Every housing cage contained no more than 5 mice, and breeding cages contained 1 male and up to 2 females. 8 weeks old females were used for primary neutrophils and CD8$^+$ T cells isolation. To induce hematopoietic-loss of SRGAP2, bone marrows from SRGAP2-deficient mice and their WT littermates were transplanted into wildtype recipient mice at 8 weeks old that had been subjected to 1000cGy X-Ray irradiation. Eight weeks later, the transplanted male and female mice were used for intravital observation or heart ischemia/reperfusion (IR) model study respectively. All animal studies were approved by the institutional animal care and use committees of Yale University.

Zebrafish

Zebrafish were of the Tu/AB background. Zebrafish were maintained as previously described (Zhang et al., 2008) according to standard protocols. Embryos were obtained through natural spawning. For the establishment of the zebrafish transgenic line expressing GFP-tagged F-BAR domain of mouse SRGAP2 in neutrophils, a fish lysozyme C (Lyz) promoter (Zhang et al., 2008) and the cDNA encoding FBAR-GFP (residues1-501) were cloned into the tol2-mpx-mCherry plasmid (29585, Addgene) (Yoo et al., 2010) by replacing the mpx-mCherry fragments. 50pg of the tol2-lyz-FBAR-GFP plasmid and 50pg tol2 transposase mRNA were coinjected into each embryo at one cell stage. About 50 injected embryos were raised to adult and subjected to screening for GFP-expressing progeny embryos according to the green positive cells pattern as previously reported (Zhang et al., 2008; Hall et al., 2007). The transgenic founder was further crossed to wild-type fish to produce the stabled transgenic line, referred to as *Tg(lyz:FBAR-GFP)*. To analyze the localization of FBAR-GFP in fish neutrophils attaching to the blood vessels, *lyz:FBAR-GFP* fish were crossed with *Tg(kdrl:mRFP)* fish (Yu et al., 2015). The double positive embryos at 3 days post fertilization (dpf) were chosen for imaging. To induce the neutrophils attachment to the vein wall, a small incision at the ventral fin of anaesthetized 3 dpf *lyz:FBAR-GFP* / *kdrl:mRFP* compound transgenic larvae was made using a sterile scalpel followed by mounting in 1% low melting point agarose (Sigma) in the E3 medium (5 mM NaCl, 0.17 mM KCl, 0.33 mM $CaCl_2$, 0.33 mM $MgSO_4$, 10-% Methylene Blue). Spinning-disk confocal microscopy was performed using the Improvision UltraVIEW VoX system (Perkin-Elmer) built on a Nikon Ti-E inverted microscope, equipped with water-immersion lenses (40X) and controlled by Volocity (Improvision) software. Embryos were kept in a heated chamber at 29°C during the whole imaging duration. In particular, the posterior cardinal vein (PCV) area above the yolk extension was illuminated. The Z stack images were acquired with plane sectioning at 0.3 μm. All animal studies were approved by the institutional animal care and use committees of Yale University.

Cell Lines

HEK293T (ATCC® CRL-3216™) cells and mouse endothelial cells (Wang et al., 2008) were cultured in Dulbecco's Modified Eagle's Medium supplemented with 10% fetal bovine serum (FBS), 4 mM L-glutamine and 100 unit penicillin and streptomycin. And cells were kept in a 5% CO2 incubator at 37°C. Transient transfection with HEK293T cells was carried out using Lipofectamine Plus (Life Technologies), and samples were collected 24 hr after transfection.

METHOD DETAILS

Neutrophil Preparation and Transfection

Murine neutrophils were purified from bone marrows as previously described (Zhang et al., 2010). Briefly, bone marrow cells collected from mice were treated with the ACK buffer (155 mM NH_4Cl, 10 mM $KHCO_3$ and 127 μM EDTA) for red blood cell lysis, followed by a discontinuous Percoll density gradient centrifugation. Neutrophils were collected from the band located between 81% and 62% of Percoll. Transient transfection of neutrophils were done as previously described (Yuan et al., 2017; Basit et al., 2016; Simunovic et al., 2015; Loison et al., 2014; Zhang et al., 2013; Tang et al., 2011; Xu et al., 2010; Zhang et al., 2010; Sun et al., 2007). In brief, three million neutrophils were electroporated with 1.6 μg endotoxin-free plasmids or 300 nM of siRNA using the human monocyte nucleofection kit (Lonza, Switzerland) with an Amaxa electroporation system. The cells were then cultured for overnight in the medium supplied with the kit containing 10% FBS and 25 ng/ml recombinant GM-CSF (PeproTech, Rocky Hill, NJ). Cell sorting was done by a FACS Aria sorter (BD, San Jose, CA).

Immunostaining and Observation of Neutrophils

Neutrophils were fixed with 4% Para-formaldehyde for 10 min and permeabilized with 0.01% saponin for 5 min and blocked with 2% BSA in PBS for 1hr. Cells were then incubated with 1:100 diluted primary antibodies in blocking buffer at 4°C for overnight. Next day, secondary antibodies with conjugated fluorescent probes (Alexa488 colored in green and Alexa633 colored in red in the figures) were 1:200 in blocking buffer and incubated with cells for 1hr at room temperature. Slides were prepared with the mounting medium containing DAPI, and imaged under a Leica SP5 confocal microscopy.

Quantification of polarization of immunostained proteins in neutrophils were done as previously described (Yuan et al., 2017). Briefly, if the florescence intensity in 25% of the cell periphery is accounted more than 50% of the total florescence intensity of the cell periphery, we call the cell polarized.

For colocalization quantification, Z stack images of consecutive optical planes spaced by 0.2 μm were acquired to cover the whole cell volume using confocal microscopy. Pearson's coefficient was determined using Imaris 7.2.3. The 3D images were reconstructed using Imaris 7.2.3 with a surface rendering model, and further adjusted with Image J (v1.48K).

For the imaging of neutrophils under suspension condition, the immunostained cells (staining in a microtube) or live cells were resuspended with CyGEL™ , and loaded onto a coverslip, then incubated for 10 min at 37°C, followed by imaging under a confocal microscope.

Flow Chamber Assay

To examine neutrophil adherence to endothelial cells under shear stress, mouse endothelial cells (Wang et al., 2008) were cultured to confluency on 10ng/ml fibrinogen (Fn) coated coverslips and treated with 50 ng/ml TNFα (Peprotech) for 4 hours at 37°C. The coverslips containing the endothelial cell layer were washed with PBS and placed in a flow chamber apparatus (GlycoTech). The WT and Srgap2 deficient neutrophils labeled with 1 μM CFSE (5-[and 6]-carboxyfluorescein diacetate succinimidyl esters) (Thermo Fisher Scientific) and 1 μM Far-Red (Thermo Fisher Scientific) respectively were mixed at 1:1 ratio, and flowed into the chamber at a shear flow rate of 1 dyn/cm^2. The adherent cells were then examined and counted under a fluorescence microscope. We alternated the labeled group in the study to completely eliminate the possibility of any influence from the dye.

To examine polarization in neutrophils adhered to polylysine (PK)-coated coverslips under shear stress, neutrophils were allowed to sediment to the coverslips for 10 min in the flow chamber. The sheer stress was gradually ramped up to 2 dyn/cm^2 for 10 min before being imaged by a confocal microscope.

ICAM-binding Assay

The assay was carried out as previously described (Konstandin et al., 2006). The ICAM-1-Fc-F(ab')2 complexes was generated by incubating Alexa Fluor® 647-conjugated AffiniPure goat anti-human Fcγ fragment-specific IgG F(ab')2 fragments (Jackson Immunobiology) and ICAM-1-Fc (100 μg/ml, R&D) at 4°C for 30 min in PBS. Neutrophils, which were resuspended at 0.5 × 10^6 cells/ml in PBS containing 0.5% BSA, 0.5 mM Mg^{2+} and 0.9 mM Ca^{2+}, were mixed with the ICAM-1-Fc-F(ab')2 complexes in the presence or absence of fMLP for 2 min. The reactions were terminated by adding 4% paraformaldehyde. After 5 min, fixation was stopped by adding 3-ml ice-cold FACS buffer (1% BSA in PBS). Cells were pelleted, resuspended in 300 μl of FACS buffer, and analyzed on a BD LSRII flow cytometer.

Integrin Blocking and Neutrophil Spreading

For blocking the integrin by the anti-integrin antibody cocktail, neutrophils were incubated with the integrin β1 and β2 antibodies (10 μg/ml each) for 30 min at RT before the assays. For neutrophil spreading assay, neutrophils were kept on the ice for 1 hour

and then placed onto Fn coated coverslips for 15 minutes. The cells were fixed with 4% paraformaldehyde and imaged under a phase contrast microscopy.

In Vitro Chemotaxis Assay in a Dunn Chamber

The chemotaxis assay using a Dunn chamber was carried out as previously described (Zhang et al., 2010). We analyzed wildtype and mutant neutrophils simultaneously by labeling the cells with different tracing dyes. We alternated the labeled group in the study to completely eliminate the possibility of any influence from the dye. Time-lapse image series were acquired at 30-second intervals for 30 mins and were analyzed using the MetaMorph image analysis software as described in (Zhang et al., 2010) . We normally obtain two parameters to quantify neutrophil chemotaxis: average directional errors and motility. The average directional error measures the angle between the cell migration direction and the gradient direction and reflects how well a cell follows the gradient. Motility is cell migration speed. MIP2 (100nM) was used as the chemoattractant in this study.

Intravital Microscopy

For intravital observations, mice were injected intrascrotally with recombinant mouse TNFα (0.5μg; R&D Systems; MN, USA) in 200 μl of saline for 4h prior to recording. To visualize neutrophils, rat monoclonal antibody RB6-8C5 against mouse Ly-6G (Gr-1) conjugated to PE (2μg in 200ul saline; Thermo Fisher Scientific, USA) was injected intravenously into the tail vein after TNFα stimulation. To visualize the vasculature of the cremaster muscle, mice were injected with 10 μg rat mAb against mouse PECAM-1 [eBioscience San Diego, CA, USA Clone 390, which has been previously reported not to interfere with leukocyte recruitment (Tasaka et al., 2003; Christofidou-Solomidou et al., 1997)] conjugated to Alexa647 (Thermo Fisher Scientific, Eugene, OR, USA). A mixture of 10 mg/kg xylazine (Bayer Inc., Animal Health, Toronto, ON, Canada) and 200 mg/kg ketamine hydrochloride (Rogar/STB Inc., Montreal, QC, Canada) was injected intraperitoneally to anesthetize mice. In all protocols, the left jugular vein was cannulated to administer additional anesthetics or antibodies. The mouse cremaster muscle was used to study neutrophil recruitment as previously described (Liu et al., 2005) with the exception that neutrophil extravasation was visualized with spinning-disk confocal microscopy using a 20x water/0.95 immersion objective to focus the excitation onto the sample (Olympus, Center Valley, PA, USA). A 512x512 pixel back-thinned electron-multiplying charge-coupled device camera (C9100-13, Hamamatsu) was used for fluorescence detection. Volocity software (Improvision) was used to acquire and analyze images. A neutrophil was considered to be adherent if it remained stationary for more than 30 s, and total leukocyte adhesion was quantified as the number of adherent cells within a 100 μm length of venule during 5 min. Rolling flux is counted via the number of leukocytes/neutrophils that pass through the 100 um/min. Leukocyte emigration was defined as the number of cells in the extravascular space within a 200x300 microns area (0.06 mm^2) adjacent to the observed venule.

Echocardiography

Transthoracic 2-dimensional M-mode echocardiogram measurements were performed to analyze cardiac function using the Vevo770 system equipped with a 35-MHz transducer (Visualsonics, Toronto, Canada). Briefly, Mice were anaesthetized with inhalation of 1.5–2% isoflurane, and the left ventricular (LV) wall thickness, LV end-systolic diameter, and LV end-diastolic diameter were measured. Percentage of fractional shortening (FS%) and ejection fraction (EF%) were calculated as described (Wasilewski et al., 2016). The measurements were performed before the surgery and at 24 hr after heart I/R.

Murine Heart Ischemia/reperfusion (IR) Models

Myocardial I/R injury was induced in mice as described previously (Wang et al., 2014). Briefly, the mice were anesthetized by 5.0% isoflurane, intubated and ventilated using a rodent ventilator. Anesthesia was maintained by inhalation of 1.5% to 2% isoflurane driven by 100% oxygen flow. Body temperature was regulated at 37°C by surface water heating. The hearts were exposed and the left anterior descending (LAD) coronary artery was ligated with an 8-0 silk ligature. After occlusion for 45 min, the coronary artery was reperfused by releasing the suture knot. 24 hours after reperfusion, the hearts were removed and perfused with saline. The infarct size was examined by TTC (2,3,5-triphenyltetrazolium chloride) staining. For TTC staining, the heart was perfused with 1% Evans Blue, and then sliced and incubated in 2% TTC for 15 min at 37 °C, and then kept in 4% PFA prior to acquiring images. Ratios of infarct size vs. ventricle area were measured and expressed as a percentage. For FACS analysis, heart was homogenized and digested in Dulbecco's Modified Eagle Medium (DMEM) medium plus 10% FBS and Penicillin-Streptomycin (50 U/mL) with 2mg/ml collagenase for 1.5h at 37°C. The single cell suspension was subjected to antibodies staining and followed by flow analysis. For the neutrophils immunohistochemistry analysis, paraffin sections with the heart after I/R procedure were prepared and stained with an anti-Ly-6B.2 antibody.

Blood Cell Counts

A Hemavet system (Drew Scientific), which is a multiparameter, automated hematology analyzer designed for in vitro diagnostic use, was used to count the leukocyte numbers in circulating blood.

Immunoprecipitation

HEK293T cells were lysed in a cell lysis buffer (20 mM Tris-HCl, pH 7.5, 150 mM NaCl, 1% NP-40, 5 mM EDTA, Roche's protease inhibitor cocktail, Roche's phosphatase inhibitor cocktail). After removing insoluble materials by centrifugation, immunoprecipitation

was carried out by adding various antibodies and Protein A/G-PLUS-agarose beads into supernatants. Immunocomplexes were washed three times with lysis buffer before the SDS sample buffer was added for SDS-PAGE analysis.

Preparation of Recombinant Proteins

His-tagged RPH3A and SRGAP2 (502-1038 aa) were expressed in E. coli BL21(DE3) and purified by affinity chromatography using Ni-NTA agarose beads (GE Healthcare). Proteins were dialyzed to a buffer containing 20 mM HEPES, pH 7.5, 100 mM KCl, 0.1% Triton X-100, 0.2 mM EGTA, 10% glycerol, and 1 mM DTT.

Buoyant Density Flotation of Liposome Assay

The assay was performed as previously described (Boswell et al., 2012) with modifications. Liposomes were consisted of 87% phosphocholine (PC) and 9% phosphatidylserin (PS), which were purchased from Avanti Polar Lipids, with or without 4% individual phosphoinositide. Liposomes were generated by sonication using a bath sonicator. They were then incubated with His-RPH3A proteins (14 μg/ml) for 30 min on ice in 75 μl of 25 mM HEPES, pH 7.4, 100 mM KCl, 10% glycerol, and 1 mM DTT (reconstitution buffer). Liposomes binding reactions were conducted in the absence of Ca^{2+} (0.2 mM EGTA) or presence of 100 μM of free Ca^{2+}. 75 μl of 80% Accudenz was added to the binding reaction to yield a final concentration of 40% Accudenz. 30% Accudenz and reconstitution buffers were then layered on top and centrifuged for 4 h in a TLA100 rotor at 32,000 rpm. The liposome layer was collected for Western analysis.

PI4KA Lipid Kinase Assay

The kinase assay was performed as previously described (Baskin et al., 2016) with modifications. Briefly, HA-tagged PI4KA protein was immunoprecipitated from HEK293T cells expressing PI4KA-HA and reconstituted in the kinase buffer (9802, Cell signaling). Liposomes containing 2μg C16-PtdIns (Echelon Biosciences) generated by sonication in the kinase buffer, γ^{33}P-labelled ATP (15 μCi), and cold ATP (50 μM) were mixed with PI4KA-HA protein and incubated with or without recombinant SRGAP2 protein for 30 min at 37°C. The reaction was quenched by the addition of 700 μl of 2:1 chloroform/methanol containing 10 μg/ml Folch fraction (brain phosphoinositides) and 400 μl of 0.1M HCl. The organic extracts were dried, resuspended in a small amount of 1:1 chloroform/methanol, and analyzed by thin-layer chromatography (mobile phase is 14:32:24:30:64 water/acetic acid/methanol/acetone/chloroform). PtdIns(4)P was quantified by autoradiography using a STORM 860 system (Molecular Dynamics).

$CD8^+$ T cells Preparation and Transfection

Murine $CD8^+$ T cells were isolated from the spleens of female mice (8 weeks old) with the $CD8^+$ T cell isolation kit according to the manufacturer's instructions (Miltenyi Biotec, 130-104-075). Primary $CD8^+$ T cells were cultured in RPMI 1640 medium (Gibco, 11875-093) supplemented with 10% FBS, penicillin (100 U/ml), streptomycin (100 μg/ml), 2-mercaptoethanol (500 μM), and HEPES (10 mM) at 37 °C in the presence of anti-CD3e (10 ug/ml) and anti-CD28 (10 μg/ml) for 24 h before transfection. Three million CD8+ T cells were electroporated with 1.6 μg endotoxin-free plasmids using Mouse T Cell Nucleofector™ Kit (VPA-1006, Lonza, Switzerland) with an Amaxa electroporation system. The cells were then cultured for overnight in the culture media provided by the kit prior to micropipette aspiration assay.

$CD8^+$ T cells Immunostaining

For immunofluorescence staining, freshly isolated CD8+ T cell were stimulated with CXCL12 (2 μM) for 30s at 37 °C min either in suspension or attached to a Fn-coated coverslip, and fixed with 4% para-formaldehyde, then followed by the same procedure as neutrophils immunofluorescence staining described above.

Micropipette Aspiration Assay

The micropipette pulling experiment was performed as previously reported (Stachowiak et al., 2014). Briefly, micropipettes with long tapers >1 cm were drawn from borosilicate capillaries (WPI, Sarasota, FL, 1 mm OD, 0.58 mm ID) using a Sutter P-1000 puller (Novato, CA). Tips were cut at 1.5-4 μm diameter using a Narishige MF-830 microforge (Tokyo, Japan) using a small molten glass bead. Observation chambers consisted of a pair of glass coverslips (#1.5, Waldemar Knittel Glasbearbeitungs-GmbH, Braunschweig, Germany) separated by 3 mm, attached to a metal block using vacuum grease. The coverslips were pretreated twice with 30% KOH in Ethanol with sonication for 5' each, followed by twice washing in sterile-filtered H_2O with sonication for 5'. The chamber and pipettes were filled with 0.5% BSA in HBSS with calcium, magnesium (14025092, Thermo Fisher). Neutrophils or $CD8^+$ cells were suspended in the same solution, and introduced into a corner of the observation chamber. Aspiration pressure was controlled using a hydrostatic system. The pressure difference between the two reservoirs was continuously read using a pressure sensor (Validyne DP-15) and transducer (Model CD223, Validyne Engineering, Northridge, CA). Gentle suction was applied with the micropipette (mounted on a Narishige MHW-3 3-axis manipulator) to pick up and lift the neutrophil above the coverslip. Time lapse images were recorded every 6 seconds with an Ultraview spinning disk confocal microscope (Perkin-Elmer Life Sciences) equipped with a Hamamatsu C9100 EM-CCD camera and Nikon TE2000-E inverted microscope, and controlled by Volocity (Improvision) software. Images were further processed using ImageJ. (v1.48K).

QUANTIFICATION AND STATISTICAL ANALYSIS

Statistical tests were performed with GraphPad Prism software (version 7.0). All data are presented as the mean ± SEM. Comparisons between multiple treatments were made using one-way or two-way Anova tests. Comparisons between the mean variables of 2 groups were made by two-tailed Student's t test. P values of $P < 0.05$ (*, $P < 0.05$; **, $P < 0.01$, ***, $P < 0.001$) were considered to indicate statistical significance. Detailed statistical information about the number of biological replicates, number of cells, and number of animals can be found in the figure legends.

Developmental Cell, Volume *49*

Supplemental Information

Leukocyte Cytoskeleton Polarization Is Initiated by Plasma Membrane Curvature from Cell Attachment

Chunguang Ren, Qianying Yuan, Martha Braun, Xia Zhang, Björn Petri, Jiasheng Zhang, Dongjoo Kim, Julia Guez-Haddad, Wenzhi Xue, Weijun Pan, Rong Fan, Paul Kubes, Zhaoxia Sun, Yarden Opatowsky, Franck Polleux, Erdem Karatekin, Wenwen Tang, and Dianqing Wu

SUPPLEMENTARY FIGURES

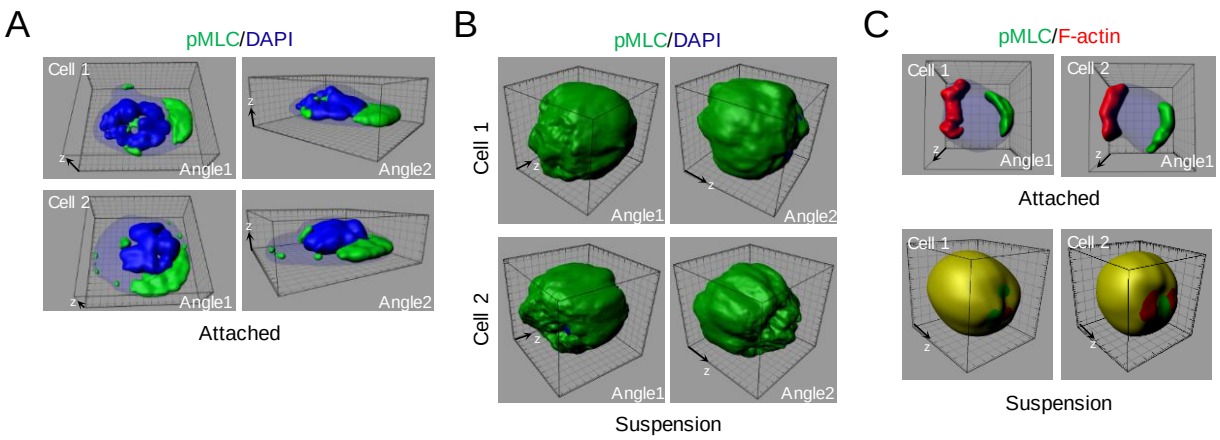

Figure S1. Neutrophil polarization requires cell attachment (Related to Figure 1).
A,B) Mouse neutrophils attached on Fn-coated coverslips (**A**) or suspended in a microtube (**B**) were stimulated uniformly with MIP2 (100 nM) for 3 min at room temperature (RT). Cells were stained with DAPI and anti-pMLC and imaged with a confocal microscope. Reconstructed 3D images of two representative cells per condition are shown. The grid scales are 1 µm. The experiments were repeated three times.
C) Primary $CD8^+$ T cells were stimulated with CXCL12 (2 µM) for 30s at 37 °C either in suspension or attached to an Fn-coated coverslip. Cells were stained with phalloidin and anti-pMLC and imaged by a confocal microscope. Reconstructed 3D images of two representative cells per condition are shown.

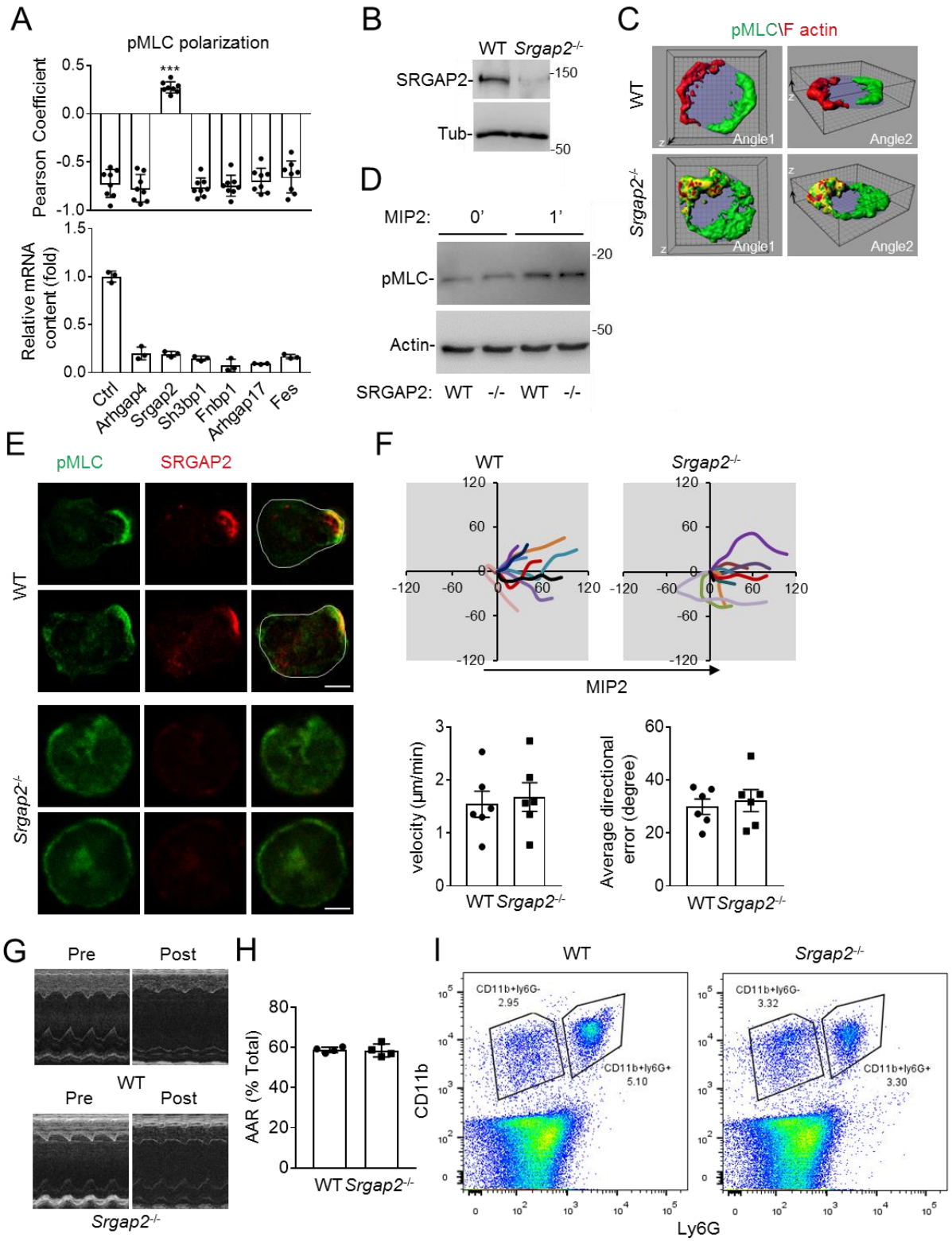
A
pMLC polarization
Pearson Coefficient
0.5
0.0
-0.5
-1.0
***
Relative mRNA content (fold)
1.5
1.0
0.5
0.0
Ctrl
Arhgap4
Srgap2
Sh3bp1
Fnbp1
Arhgap17
Fes
B
WT
Srgap2-/-
SRGAP2-
-150
Tub-
-50
C
pMLC\F actin
WT
Srgap2-/-
Angle1
Angle2
D
MIP2:
0'
1'
pMLC-
-20
Actin-
-50
SRGAP2:
WT
-/-
WT
-/-
E
pMLC
SRGAP2
WT
Srgap2-/-
F
WT
Srgap2-/-
120
60
0
-60
-120
MIP2
velocity (μm/min)
Average directional error (degree)
WT
Srgap2-/-
G
Pre
Post
WT
Srgap2-/-
H
AAR (% Total)
80
60
40
20
0
WT
Srgap2-/-
I
WT
Srgap2-/-
CD11b+ly6G-
2.95
CD11b+ly6G+
5.10
CD11b+ly6G-
3.32
CD11b+ly6G+
3.30
CD11b
Ly6G

Figure S2. Importance of SrGAP2 in neutrophil polarization and adhesion (Related to Figure 2).

A) SiRNA screen for BAR domain-containing proteins that is important for pMLC polarization. Neutrophils were transfected with one of the siRNAs and the GFP cDNA. GFP-positive cells were isolated by FACS and subjected to stimulation and staining as Fig. 1A. Colocalization of pMLC and F-actin is quantified (upper panel). Target mRNA was determined by quantitative RT-PCR (lower panel). Data are presented as means ± SEM. Each data point in the upper panel represents one cell (***, $p<0.001$ vs control; One-way Anova). Ctrl, control.

B) Western analysis of neutrophils with an SRGAP2 (G10) and an anti-β-tubulin (Tub) antibody.

C) Another sets of cells for Fig. 2A.

D) Western analysis of neutrophils stimulated with MIP2 (100 nM) with anti-pMLC and anti-beta actin.

E) Validation of specificity of the anti-SRGAP2 antibody in immunostaining. WT and Srgap2$^{-/-}$ neutrophils were stimulated as in Fig. 1A and stained by the anti-pMLC and anti-SRGAP2 (C14). Scale bar is 3 μm. The experiments were repeated three times.

F) SRGAP2-deficiency does not affect chemotaxis. Neutrophil chemotaxis was assessed in a Dunn chamber with a MIP2 gradient. Representative cell migration traces as well as quantitative chemotactic parameters are shown. Data are presented as means ± SEM. Each data point represents the average of more than 15 cells per experiment. The experiments were repeated five times.

G) Representative echocardiograms for Figure 2H. Pre, pre-ischemia/reperfusion (IR) procedure; Post, 24 hr after IR procedure.

H) SRGAP2-deficiency does not affect area at risk (AAR) over the area of the ventricle.

I) Representative flow cytometry plots for Figure 2K.

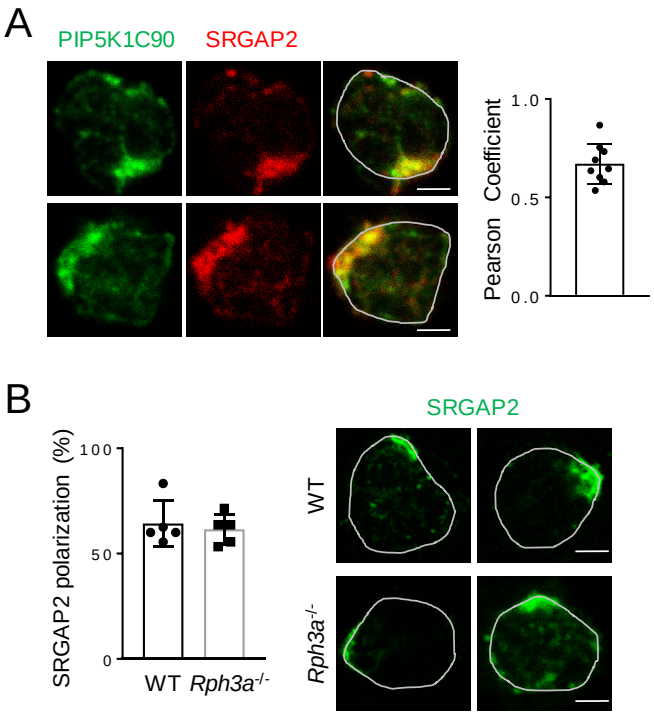

Figure S3. RPH3A-deficiency does not affect SrGAP2 polarization, which is colocalized with PIP5K1C90 (Related to Figure 3).
A) Neutrophils were treated as in Fig. 1A before being stained with anti-PIP5K1C90 and anti-SRGAP2 (G10) antibodies. Representative optical section images of two cells are shown. Data are presented as means ± SEM. Each data point represents one cell. The experiments were repeated three times.
B) Neutrophils were stimulated as in **A** before being stained with the anti-SRGAP2 (G10) antibody. Representative optical section images of two cells from each genotype are shown. Data are presented as means ± SEM. Each data point represents the average of more than 10 cells per observation field, and the experiment was repeated five times.
Scale bars are 3 µm.

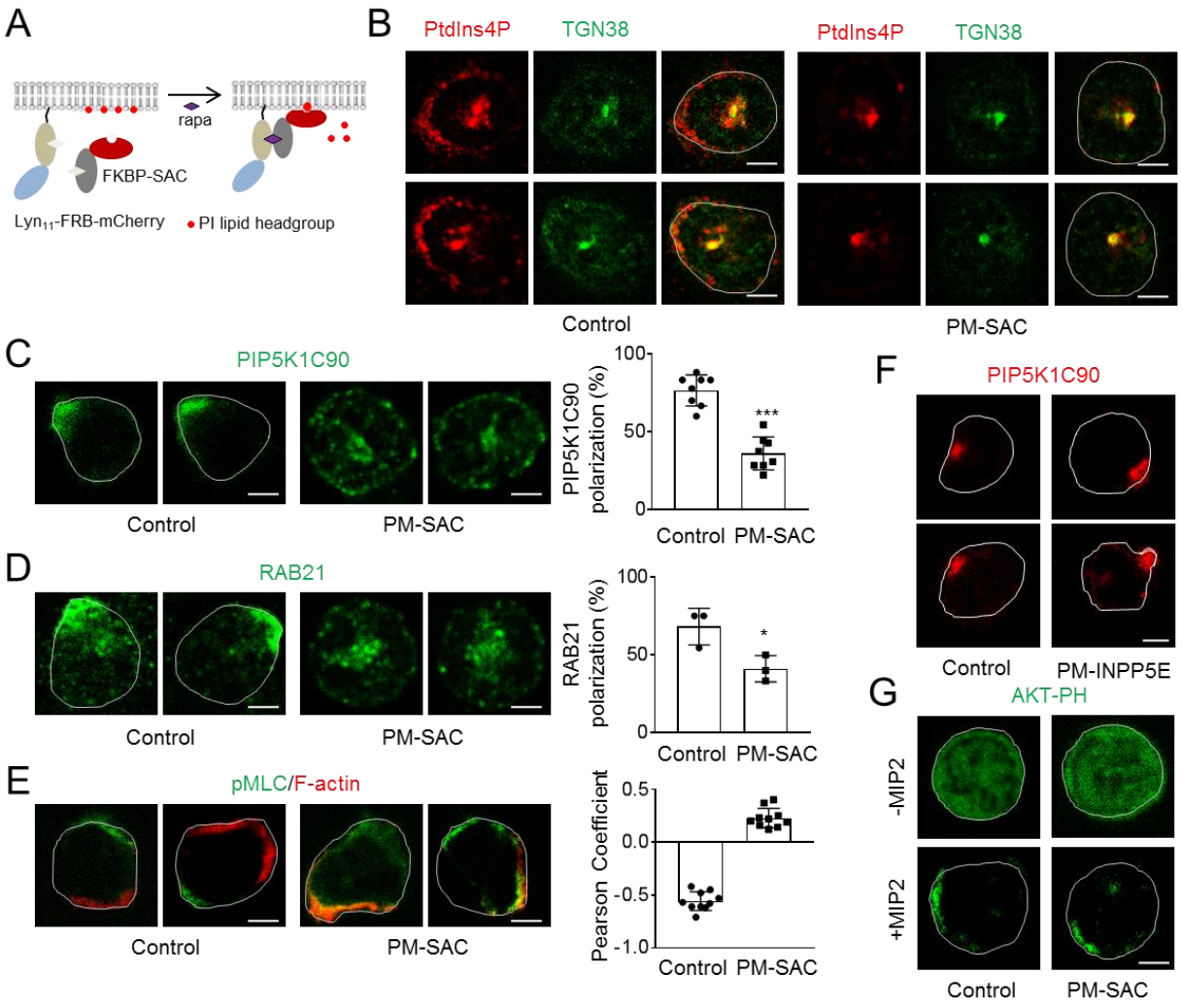

Figure S4. Effects of PM PtdIns4P depletion (Related to Figure 4).
A) Schematic representation of the rapamycin-induced PM PtdIns4P depletion system.
B) Validation of the rapamycin-induced PM PtdIns4P depletion system and anti-PtdIns4P antibody. Neutrophils were prepared and stimulated in the presence of 1 μM rapamycin as in Fig. 4D, before being stained with anti-PtdIns4P and anti-TGN38, followed with Alexa633 and Alexa488 conjugated secondary antibodies, respectively. The system selectively depletes PM PtdIns4P detected by immunostaining with an anti-PtdIns4P antibody without obvious effects on the Golgi PtdIns4P.
C-E) Depletion of PtdIns4P impairs polarization of PIP5K1C90, RAB21, and pMLC. Neutrophils were prepared and stimulated in the presence of 1 μM rapamycin as in Fig. 4D before being stained with anti-PIP5K1C90 or anti-RAB21 antibody and an Alexa488-conjugated secondary antibody (**C,D**) or with Alexa633-phalloidin (for staining F-actin) and anti-pMLC followed with an Alexa488-secondary antibody (**E**). Representative optical section images of two independent cells from each condition are shown. Data are presented as means ± SEM (***, $p<0.001$; *, $p<0.05$; two-tailed Student's t-Test). Each data point represents the average of more than 15 cells per observation field, and the experiment was repeated four times.
F) Depletion of PtdIns4,5P_2 has no effect on PIP5K1C90 polarization. Neutrophils were transfected with Lyn_{11}-FRB-mCherry and FKBP-INPP5E at 1:5 ratio and separated into mCherry

positive (PM-INPP5E) and negative (Ctr) pools by FACS. These neutrophils were then stimulated as in Fig. 1A in the presence of 1 μM rapamycin before being stained with anti-PIP51C90 and Alexa633-conjugated secondary antibody. Representative optical section images of two cells from each condition are shown.
G) Depletion of PtdIns4P has no effect on localization of AKT-PH-GFP in neutrophils. Neutrophils were transfected with Lyn_{11}-FRB-mCherry, FKBP-SAC and AKT-PH-GFP and separated into GFP/mCherry positive (PM-SAC) and GFP only (Ctr) pools by FACS. These neutrophils were treated with 1 μM rapamycin and placed on Fn-coated coverslip in the presence or absence of MIP2 for 3 min before examined by a confocal microscope.
Scale bars for all images are 3 μm.

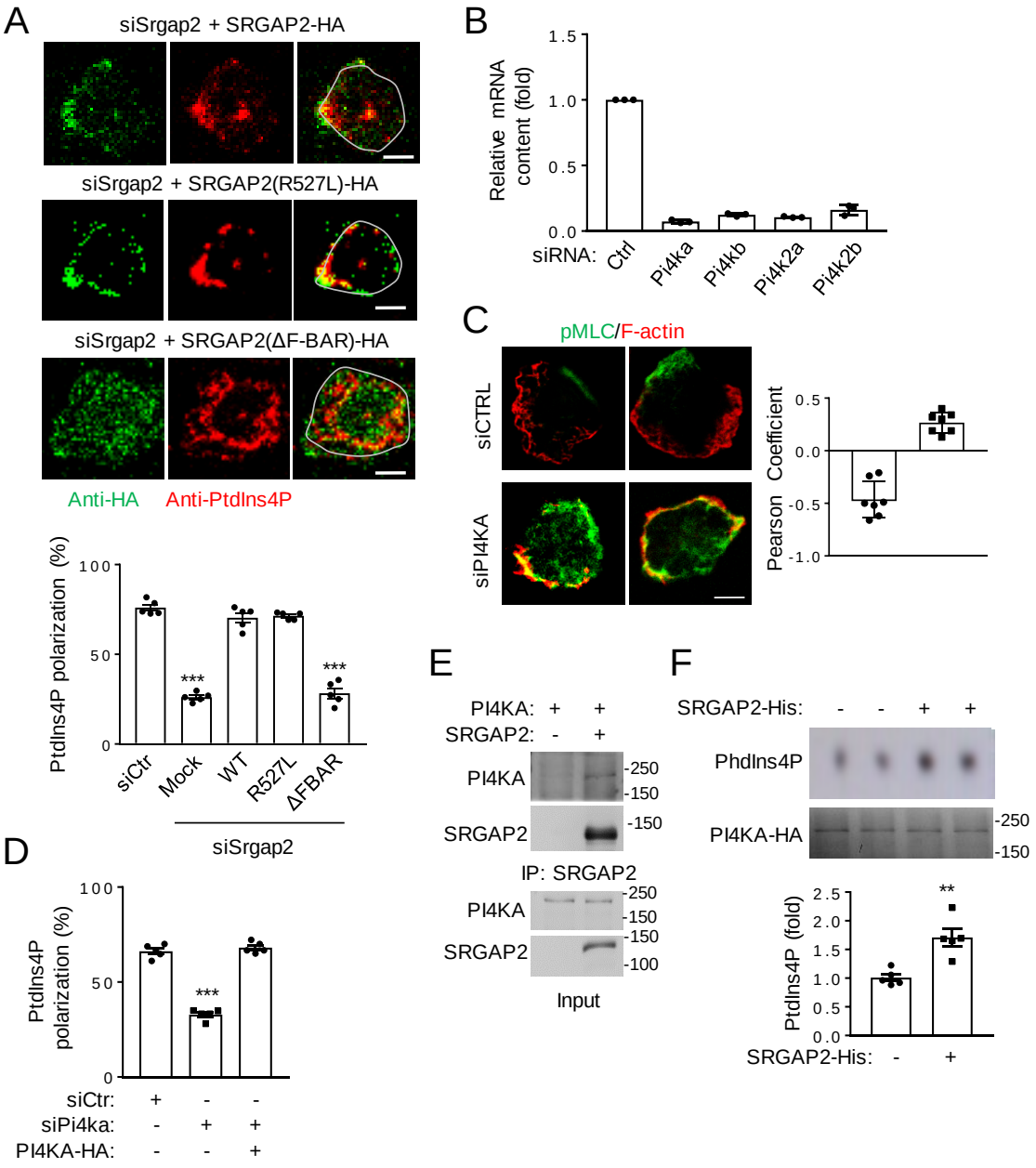

Figure S5. Involvement of PI4KA (Related to Figure 5).
A) Re-expression of WT SRGAP2 or R527L, but not ΔF-BAR mutant, restore PtdIns4P polarization. The cells were detected by anti-PtdIns4P and anti-HA antibodies. Data are presented as means ± SEM (***, p<0.01; two-tailed Student's t-Test). Each data point represents the average of more than 15 cells per observation field.
B) Validation of siRNA efficiency by qRT-PCR.
C) PI4KA knockdown impairs pMLC polarization in neutrophils.
D) Effect of PI4KA knockdown is rescued by expression of human PI4KA cDNA in mouse neutrophils. Neutrophils were transfected with siRNA and cDNA as indicated and stimulated as Fig. 1A. Cells were stained with anti-PtdIns4P and the Alexa633 secondary antibody. Data are presented as means ± SEM (***, p<0.001; One-way Anova). Each data point represents the average of more than 10 cells per observation field, and the experiment was repeated twice.

E) Co-immunoprecipitation of SRGAP2-HA and PI4KA-Myc in HEK293 cells overexpressing these two proteins. Immunoprecipitation was carried out by using an HA antibody. The experiments were repeated three times.
F) SRGAP2 recombinant protein stimulates the lipid kinase activity of PI4KA precipitated from HEK293 cells overexpressing PI4KA in an in vitro kinase assay. A representative phosphoimage is shown. Data are presented as means ± SEM (**, $p<0.01$; two-tailed Student's t-Test). Each data point represents a biological replicate.

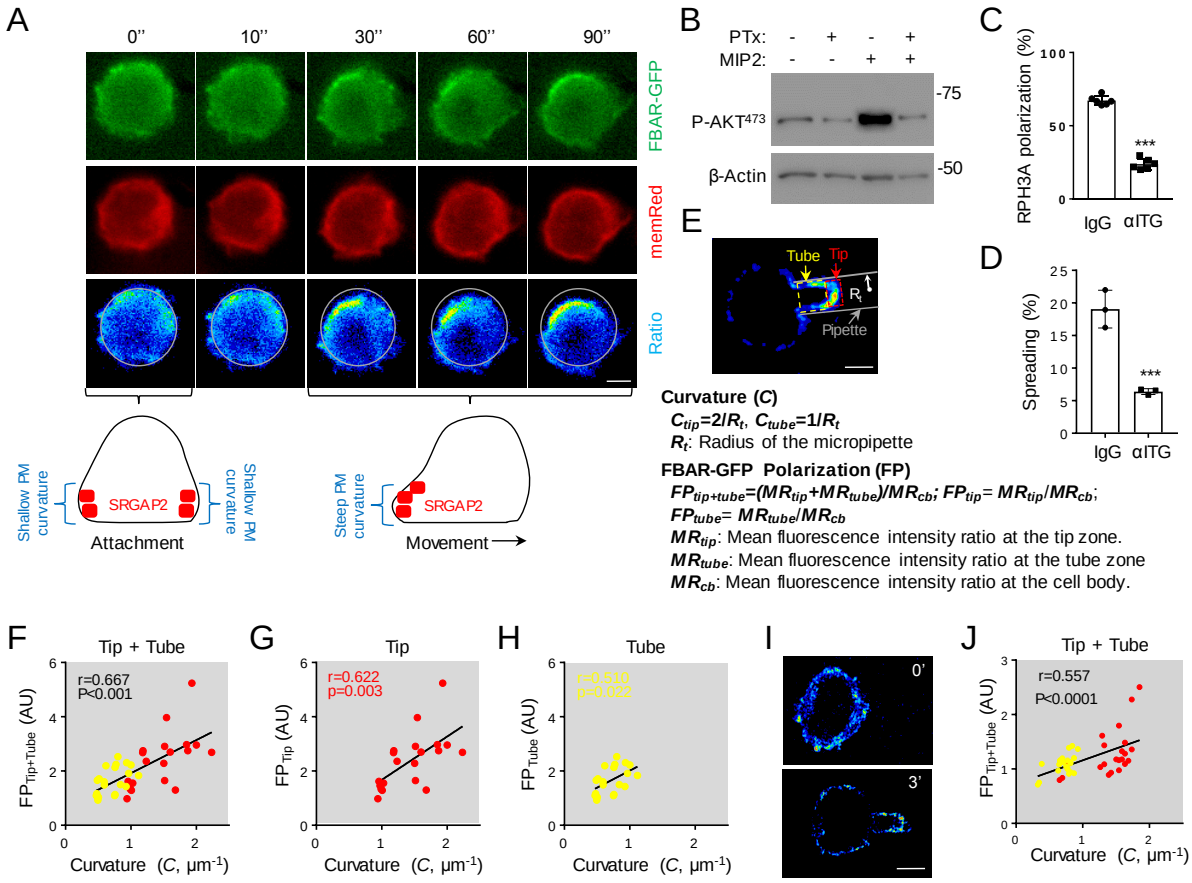

Figure S6. Mechanism for SRGAP2 F-BAR-domain polarization (Related to Figure 6).
A) Real time detection of F-BAR-GFP polarization. MemRed expressing neutrophils from mT/mG mouse were transfected with F-BAR-GFP. The cells were placed onto PK-coated coverslips to let them settle down on the surface by gravity. Images were acquired at a 10 sec internal. Serial images of a cell that is representative for those drifting or slowly moving on the coverslip are shown. The position of the cell at Time 0 is marked by the circle. The experiments were repeated five times. Schematic explanation for anteroposterior polarization of FBAR-GFP in this cell is also provided.
B) Effect of PTx on MIP2-stimualted phosphorylation on AKT in neutrophils. Neutrophils were pretreated with 1 μg/ml of PTx for 2 hr at 37°C, followed by stimulation with 100 nM MIP2 for 1 min before Western analysis.
C-D) Effects of the anti-integrin cocktail on RPH3A polarization and neutrophil spreading. Neutrophils were placed on Fn for 30 min in the presence of control IgG or anti-β1 and β2 integrin (10 μg/ml). Cells were stained for anti-RAPH3A (**C**) or imaged for spreading by phase-contrast microscopy (**D**). Data are presented as means ± SEM (***, p<0.001; two-tailed Student's t-Test). Each data point represents average of more than 10 cells per observation field. The experiments were repeated twice.
E) Schematic representation for quantification of PM curvature and FBAR-GFP polarization (FP).
F-H) Correlation of PM curvature within the pipette with FBAR-GFP polarization.
I,J) PM curvature-dependent recruitment of SRGAP2 F-BAR-GFP in primary $CD8^+$ T cells. Experiments and analysis were done as in **E,F**.
Scale bars (**A, E, I**) are 3 μm.

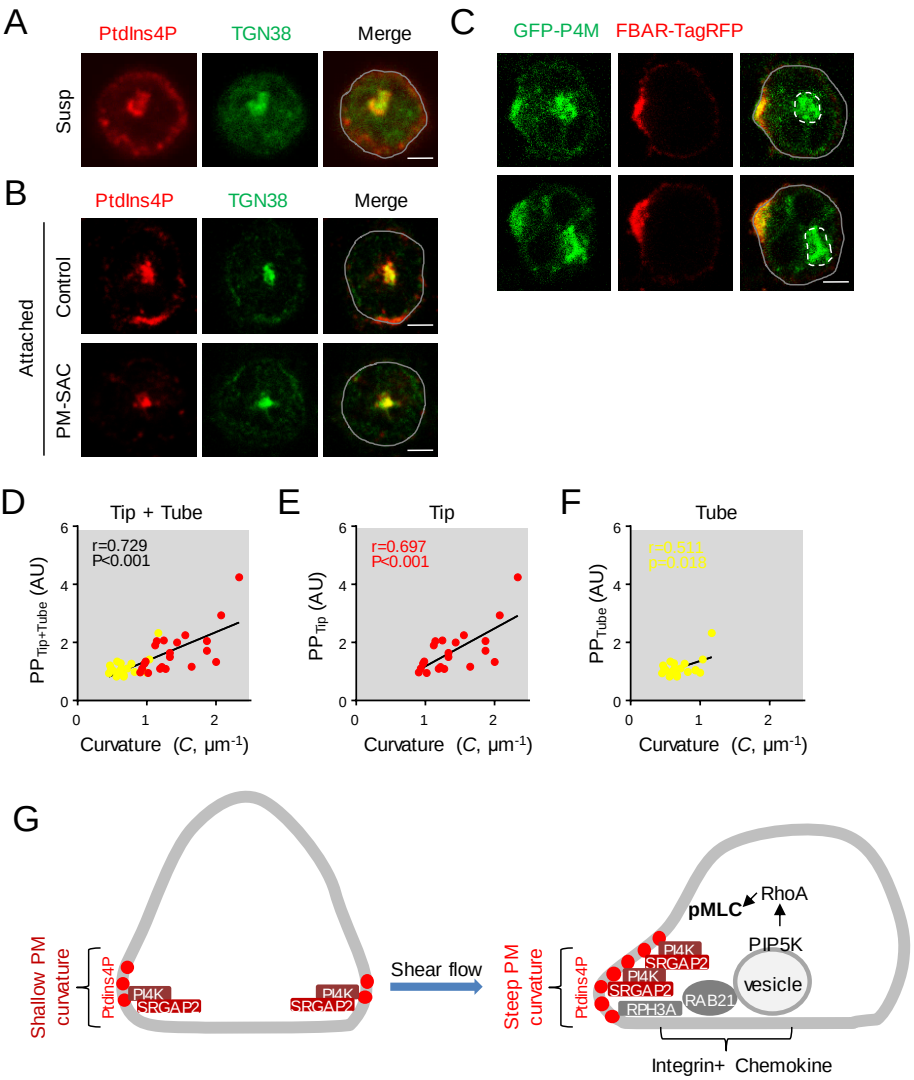

Figure S7. Mechanisms for membrane curvature to induce PtdIns4P polarization and underlie chemical-induced neutrophil polarization (Related to Figure 7).

A-B) Cell attachment induces PtdIns4P polarization. Neutrophils were fixed in suspension (A) or after attached to PK-coated coverslips (**B**). Cells in **B** were transfected with the PM-PtdIns4P depletion system and treated with rapamycin as in Fig. 4D. Cells were stained with anti-PtdIns4P and anti-TGN38 antibody, followed by Alexa633 (red) and Alexa488 (green) conjugated secondary antibodies, respectively. Representative optical section images are shown. Scale bars are 3 μm. The experiments were repeated five times.

C) Co-polarization of GFP-P4M and FBAR-TagRFP in neutrophils attached to PK-coated surface. Neutrophils were transfected with GFP-P4M and FBAR-TagRFP and attached to PK-coated coverslips. Representative optical section images are shown. Scale bars are 3 μm.

D-F) Correlation of PM curvature with GFP-P4M polarization. P4M polarization (PP) was calculated in the same way as FBAR-GFP polarization (FP) in Fig. S6E. The zone division and PM curvature were also calculated as depicted in Fig. S6E.

G) A model depicting the mechanism by which cell attachment-induced PM curvature induces polarization of SRGAP2 and PtdIns4P, which in turn dictates the uropod polarization of PIP5K1C90 and subsequent pMLC. The membrane curvature-dependent events are depicted in red/purple colors, whereas chemical-stimulated events are depicted in black/gray colors. Cell

attachment-induced PM curvature initially induces dorsoventral SRGAP2 polarization and subsequent PtdIns4P polarization at the cusp of cell attachment. Lateral drifting during cell settlement in *in vitro* experiments or shear flow in *in vitro* or *in vivo* experiments alters cell shape and creates steeper PM curvature at the trailing end of cell movement or flow direction, which leads to anteroposterior polarization of SRGAP2 and PtdIns4P. PtdIns4P is targeted by RAP3A, leading to polarized transport of RAB21 vesicles, which carries PIP5K1C90. PIP5K1C90 polarization leads to polarized RhoA activation and pMLC polarization. RAB21 vesicle transport, RHOA activation, and MLC phosphorylation also require integrin and chemoattractant stimulation.

Table S1. Leukocyte numbers in peripheral blood (Related to Figure 2)

	Cells x 1000 (Mean±SD)	
	WT (n=4)	*Srgap2*$^{-/-}$ (n=4)
Leukocytes	19.91±3.59	24.18±3.92
Neutrophils	4.24±1.26	4.58±0.95
Lymphocytes	13.27±2.1	17.26±2.80
Monocytes	1.69±0.19	1.21±0.32
Eosinophils	0.50±0.17	0.82±0.41
Basophils	0.21±0.06	0.32±0.11
Platelets	307.5±75.1	395.3±262.7